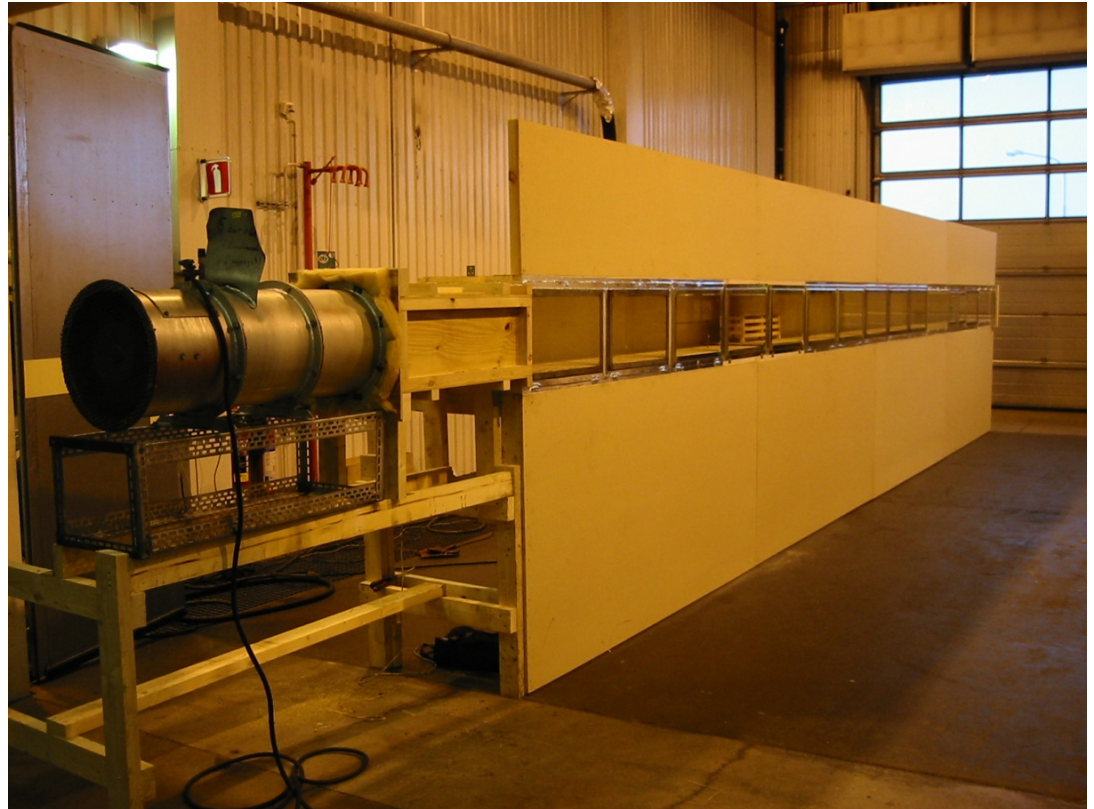


Maximum Ceiling Temperature in a Tunnel Fire

Ying Zhen Li and Haukur Ingason

SP Technical Research Institute of Sweden



Maximum Ceiling Temperature in a Tunnel Fire

Ying Zhen Li and Haukur Ingason

Abstract

Maximum Ceiling Temperature in a tunnel fire

This report focuses on the maximum excess gas temperature beneath the ceiling, and its position relative to the centre, in a tunnel fire. Effects of different ventilation systems and ventilation velocities, heat release rates, tunnel geometries and fire sources are analysed. Numerous model scale tests and most of the large scale tunnel fire tests that have been performed worldwide to date are presented.

Maximum excess gas temperature data from both model scale and large scale tests are used and analysed. Correlations for the calculation of the maximum ceiling excess gas temperature in the vicinity of the fire source, and its location relative to the centre of the fire source, are proposed for low and high ventilated tunnels. The data indicate two regions, depending on the dimensionless ventilation velocity. Each can be subdivided into two regions. The first region exhibits linear increase which transits into a constant period, depending on the fire size and ventilation.

The maximum excess gas temperature is found to be 1350 °C. Analysis of the inclination of the flame resulted in a definition and correlation for a critical flame angle. Based on these results, a correlation was obtained to calculate the position of the maximum gas temperature beneath the ceiling.

Key words: maximum temperature, position, flame angle, model scale, large scale, heat release rate, ventilation velocity, effective tunnel height

**SP Sveriges Provnings- och
Forskningsinstitut**
SP Rapport 2010:51
ISBN 91-85303-82-8
ISSN 0284-5172
Borås 2009

**SP Swedish National Testing and
Research Institute**
SP Report 2010:51

Postal address:
PO Box 857,
SE-501 15 BORÅS, Sweden
Telephone: +46 33 16 50 00
Telex: 36252 Testing S
Telefax: +46 33 13 55 02
E-mail: info@sp.se

Table of Content

1	Introduction	8
2	Theoretical Analysis	10
2.1	Interaction of ventilated flow with fire plume	10
2.2	Fire plume mass flow rate in a ventilated flow	11
2.3	Formulas for standardized time-temperature curves	12
2.4	Maximum excess gas temperature beneath ceiling	13
2.4.1	Small fire	13
2.4.2	Large fire	15
2.5	Positions of maximum temperature beneath tunnel ceiling	18
2.5.1	A short review	18
2.5.2	Small fire	19
2.5.3	Large fire	21
2.5.4	Critical flame angle	22
3	Discussion of results	24
3.1	Maximum excess temperature beneath tunnel ceiling	24
3.1.1	Model scale tests	24
3.1.2	Large scale tests	25
3.1.3	Analysis of the constant regions	27
3.1.4	Formulae for maximum excess temperature	31
3.1.5	Comparison with transient tests data	32
3.1.6	Example on how to use the temperature correlation	37
3.2	Positions of maximum temperature beneath tunnel ceiling	39
3.2.1	Positions of maximum temperature	39
3.2.2	Critical flame angle	41
3.2.3	Comparison with Raj et al's formulae	42
3.2.4	Comparison with Kurioka's formulae	43
4	Conclusions	44
5	References	46
Appendix A	Model scale tests	49
Appendix B	Large scale tests	60

Preface

This project was sponsored by the Swedish Fire Road Administration (SRA) through the FUD-BT programme. We would like acknowledge Mr Bernt Freiholtz at SRA for his advice and encouragement in this project.

Summary

An analysis of the maximum excess gas temperature and its position in a tunnel fire was carried out. Large amounts of data from model scale tests and large scale tests were used to verify and improve the proposed correlations. These correlations are unique, and the need for this type of engineering correlations has been eagerly awaited.

Results of both theoretical analysis and experimental data show that the maximum temperature can be divided into two regions according to the dimensionless ventilation velocity. The dimensionless ventilation velocity is defined as the ratio of the longitudinal ventilation velocity and the characteristic plume velocity. The main parameters taken into account in the theoretical analysis include the heat release rate, the ventilation velocity, the effective tunnel height and the geometry of the fire source. For a small fire in a tunnel, the maximum excess gas temperature beneath the tunnel ceiling increases linearly with the heat release rate and decreases linearly with the longitudinal ventilation velocity when the dimensionless ventilation velocity exceeds 0.19. When the dimensionless ventilation velocity is ≤ 0.19 , the maximum gas excess temperature beneath the tunnel ceiling varies as two-thirds the power of the heat release rate, independent of the longitudinal ventilation velocity. In both regions, the maximum gas excess temperature varies as a $-5/3$ power law of the effective tunnel height, i.e. the distance between the bottom of the fire source and the tunnel ceiling.

For a large fire in a tunnel, i.e. one where the flame impinges on the ceiling and extends along the tunnel ceiling, it is found that the maximum excess temperature beneath the ceiling approaches a constant value, regardless of the ventilation velocity. However, the thermal properties of the tunnel structure, the influence of the water dripped and flowed from cracks in blasted rock tunnels, the duration of the high temperature (for example high heat release rate and low ventilation velocity) and the fuel type are all parameters that can influence the specific value of the maximum temperature in any given tunnel for any given scenario. This means that the maximum temperature in the constant regions is not a universal constant, but dependent on the specific conditions for a given tunnel fire.

Based on a theoretical model and analysis of the experimental data, a correlation for the maximum temperature beneath the tunnel ceiling is proposed. The correlation is valid up to a maximum excess gas temperature of 1350 °C. This value was found to be the upper limit for the maximum temperature obtained from large scale tunnel tests. It is, however, clear that the levels of maximum gas temperatures depend mainly on the heat release rate, the effective tunnel height (i.e. the height between the ceiling and the bottom of the burning object if the fire source is elevated from the road surface), and the ventilation type and velocity. Other factors that are less dominating but nonetheless important when determining the level of the maximum ceiling temperature are the type of tunnel linings or tunnel construction (i.e., rock, concrete, cracked and leaky blasted rock) and the fuel type. The width of the tunnel was not found to be an important parameter, and therefore not included in the correlations. The correlations are mainly based on test data from rectangular shape cross-sections, but there are also other types included. When using the correlations in tunnels that do not have rectangular shape cross-section the height at respective location should be applied.

The fuel type can be divided into vehicles, solid fuels or liquid fuels. Open solid fuels with no coverage or open liquid fires, are found to yield the highest maximum ceiling gas temperatures if the heat release rates are high enough. In the case of vehicles, the different types of exterior body types, such as steel, aluminum or glass fibre, may affect the amount of convective and radiant heat transported towards the ceiling. This, in turn, may affect the final value of the maximum ceiling gas temperature for the same level of

heat release rates. Finally it was found that the gas temperatures in model scale tests do not result in values higher than 1100 °C. This is related to the specific test conditions and thermal exchange between the fire and the material used in these model scale tests.

A formula for predicting the position of the maximum temperature beneath the ceiling was proposed based on a theoretical analysis. A flame angle in a longitudinal flow was defined from the position of the maximum temperature beneath the tunnel ceiling. The flame angle defined here is also related to the dimensionless ventilation velocity. The flame angle appears to be insensitive to the heat release rate for large tunnel fires. A critical flame angle was found, which is defined as the flame angle at the critical condition when the back-layering just disappears. This means that for a given tunnel and fire source, the flame angles under critical condition are almost of the same, independent of the heat release rate.

A comparison of the proposed formulae for the maximum temperature beneath the tunnel ceiling with transient data from model scale tests and large scale tests shows a good agreement. This means that the maximum temperature beneath the ceiling in a tunnel fire can be estimated well if the heat release rate curve and the specific geometries of tunnel and fire source are known. The good correlation, between the proposed formulae for the maximum excess temperature beneath the ceiling and its position in a tunnel fire and the data from model scale tests and large scale tests, confirm the validity of the theoretical analysis.

This page intentionally left blank.

1 Introduction

The stability of the tunnel structure is a key design parameter when concerning the fire safety design of tunnels. For example a tunnel may be the key transportation line between two countries as in the case of the Mont Blanc fire or the St:Gotthard tunnel fire [1]. A large fire can jeopardize the tunnel construction if the fire becomes too intense over a long period of time. Our knowledge concerning the impact of thermal exposure of the fire on the tunnel construction and how to calculate the stability of the structure is, therefore, critical. Traditionally, heat exposure to a tunnel construction is based on the use of standardized time-temperature curves. Indeed, standard fire temperature curve, such as ISO 834 [2], the hydrocarbon curve (HC) [3] or the RWS curve [4], are widely used to test the surface temperatures of the tunnel linings, see Figure 1.

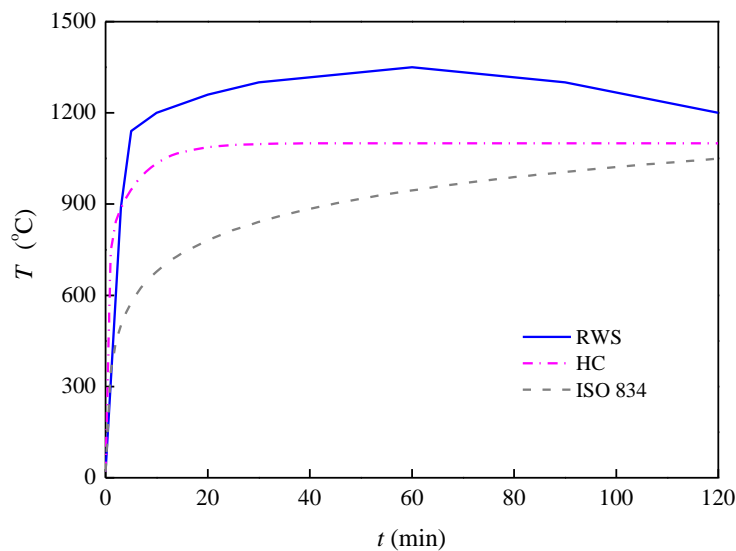


Figure 1 The most common standardized time-temperature curves for road tunnel applications.

Other time-temperature curves that are used in specific applications include RABT/ZTV [5], HCM [6] and EBA [7]. All these curves are derived in different ways and usually based on large scale or small scale tests or by agreements of technical committees working nationally or internationally in this field. When choosing different curves, there is no single guideline document concerning how to choose one curve in relation to the heat release rates, longitudinal ventilation velocity or the ceiling heights compared to others.

Therefore there is a need to develop an alternative to standardized time-temperature curves, i.e. engineering correlations to calculate the maximum gas temperature beneath the ceiling of a tunnel. Traditionally tunnel engineers use the standardized time-temperature curves to design the load bearing system of the tunnel construction. The system is designed from an arbitrarily chosen standardized time-temperature curve that is used as input for calculation of the temperature distribution inside the structure. The temperature is converted into heat flux towards the construction and the temperature inside the construction is calculated as a function of the distance from the outer surface of the construction. In the case of a concrete tunnel construction, the temperatures in the reinforced steel bars are calculated. When the temperature reaches a certain critical value the time to collapse is determined. This method is accepted by most authorities around

the world and means that the analysis will be critically dependent on the choice of the time-temperature curve.

There is, therefore, a need to develop an engineering tool based on theoretical analysis that can predict the gas temperature as a function of the tunnel geometry, heat release rate and ventilation conditions. Kurioka et al [8] proposed an empirical equation to predict the maximum gas temperature rise below the tunnel ceiling and its position relative to the centre of the fire. Hu et al [9] compared Kurioka's equation with their full-scale data and showed that there was a good agreement. However, the heat release rates of Hu's full-scale tests [9] were too small compared to the tunnel geometry. In the equation given by Kurioka et. al. the maximum gas temperature rise below the ceiling approaches infinite, when the ventilation velocity approaches zero. The consequence will be that the maximum gas temperature rise below the ceiling cannot be predicted correctly when the ventilation velocity is very low. Further, the maximum gas temperatures from Kurioka's experiments tends to be high, as the tunnel ceilings were lined with thick fireproof blankets, similar to adiabatic boundaries, which could underestimate the heat loss near the fire sources. The consequence may be that the maximum gas temperature rise under the tunnel ceilings will be overestimated. Moreover, the proposed correlation was originally obtained by empirical correlations and not based on theoretical analysis.

Li et al. conducted a theoretical analysis of the maximum gas temperature rise below the ceiling based on an axisymmetric fire plume theory [10]. The necessary empirical coefficients were obtained from experimental data. The proposed formulae for the maximum excess gas temperature beneath the ceiling fit the data from both model scale tests and large scale tests. A comparison of the proposed formulae with the Kurioka's equation was also made. The results showed that the formulae proposed by Li are better able to predict the maximum gas temperature, especially when the ventilation velocity is very small. However, the proposed formulae may not be valid if the heat release rate is so large that the combustion zone reaches up to the tunnel ceiling. If this occurs, the maximum gas temperature was expected to be a constant independent of the heat release rate, ventilation velocity and tunnel height.

In the present report the theory of the plume mass flow rate and maximum temperature beneath the ceiling for a small fire in a tunnel as given by Li et al [10] is further developed. For a large fire in a tunnel, the parameters influencing the maximum temperature are analyzed, according to theoretical considerations and tests data. Different ventilation systems, heat release rate, ventilation velocity, geometry of the tunnel and fire source are all taken into account. Data from numerous model scale tests and large scale tests have been used in the analysis. The theoretical analysis provides the basis for an engineering model to calculate the maximum gas temperature depending on the ventilation conditions, tunnel geometry and fuel characteristics.

The work by Kurioka et. al. [8] concerning the position of the maximum temperature is of great interest for the present study. The position of the maximum temperature beneath the ceiling in a ventilated tunnel fire is very important when predicting the activation of the detection system and automatic sprinkler system in a tunnel, and estimating the fire characteristics in the vicinity of the ceiling. A theoretical approach to determine the position has therefore been carried out and compared to available model scale test data.

2 Theoretical Analysis

In order to establish necessary engineering correlations for the calculation of the maximum excess gas temperature and its position relative to the fire source, a basic theoretical analysis has been carried out. The theory is explained in this chapter.

2.1 Interaction of ventilated flow with fire plume

Hoult *et al.* [11][12] made a theoretical analysis of the fire plume in a ventilated flow based on the following assumptions:

- (1) The velocity and temperature defect profiles have the shape of a top hat and that the cross section of the plume is circular.
- (2) The plume is slender, i.e. the radius is small compared to the centreline radius of curvature.
- (3) There are basically two entrainment mechanisms, i.e. that due to the difference between the plume velocity u and wind velocity component $V \cos \theta$ parallel to the plume and that due to the wind velocity component $V \sin \theta$ normal to the plume. The two mechanisms are additive.
- (4) The net rate of entrainment is the product of a dimensionless entrainment coefficient times the perimeter of the plume cross section times the corresponding velocity difference.
- (5) The entrainment coefficients α and β are independent of position along the plume.

Based on this model the fire plume with an initial radius b_{f0} goes up and is deflected by the horizontal ventilated flow, as shown in Figure 2.

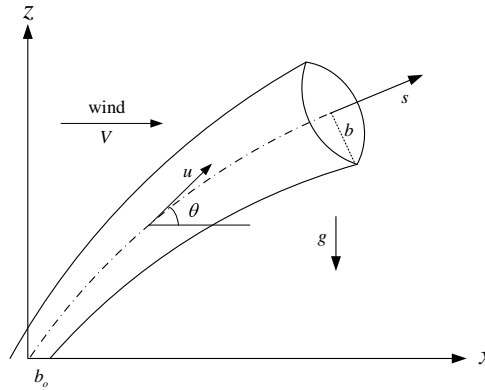


Figure 2 A diagram of the interaction of ventilated flow with fire plume.

The governing equations can be described as follows:

Mass:

$$\frac{d}{d\xi}(B^2U) = 2B[\alpha|U - V' \cos \theta| - \beta|V' \sin \theta|] \quad (1)$$

Momentum:

$$\pi \frac{d}{d\xi}(B^2U^2) = \frac{\sin \theta}{U} + \pi V' \cos \theta \frac{d}{d\xi}(B^2U) \quad (2)$$

$$\pi B^2 U^2 \frac{d\theta}{d\xi} = \frac{\cos\theta}{U} - \pi V' \sin\theta \frac{d}{d\xi} (B^2 U) \quad (3)$$

Energy:

$$B^2 U \phi = \frac{1}{\pi} \frac{u^{*2}}{b_{fo} g} \quad (4)$$

The dimensionless parameters are defined as follows:

dimensionless plume radius: $B = b / b_{fo}$,

dimensionless plume velocity: $U = u / w^*$,

dimensionless ventilation velocity: $V' = V / w^*$,

dimensionless plume temperature: $\phi = (T - T_o) / T_o$,

dimensionless position along the trajectory: $\xi = s / b_{fo}$.

The characteristic plume velocity w^* is defined as:

$$w^* = \left(\frac{gQ}{b_{fo} \rho_o c_p T_o} \right)^{1/3} \quad (5)$$

where b_{fo} is the radius of the fire source, u is the plume velocity, V is ventilation velocity, s is the trajectory, b is the radius of the fire plume at a given position, g is the acceleration of gravity, Q is the heat release rate, ρ_o is the ambient density, c_p is the heat capacity, T_o is the ambient temperature, θ is the angle between plume axis and horizontal, α is the tangential entrainment coefficient and β is the normal entrainment coefficient.

The above equations show that the plume characteristic velocity is a very important parameter in the interaction between the ventilated flow and the fire plume, with which both the dimensionless ventilation velocity and the dimensionless plume velocity are correlated.

2.2 Fire plume mass flow rate in a ventilated flow

A simple theoretical analysis to predict the maximum ceiling temperature in a longitudinally ventilated tunnel flow is given. In order to do that, we assume that we can exclude the virtual source term in the axisymmetric fire plume analysis. The virtual source term is used to compensate for the difference between the actual fire source and the ideal point source [13]. The mass flow rate of an axisymmetric fire plume in the open can then be expressed as [14][15]:

$$m_{p,o}(z) = 0.071 Q_c^{1/3} z^{5/3} \quad (6)$$

where Q_c is the convective heat release rate, z is the height.

Normally in a longitudinally ventilated tunnel, the fire plume on the downstream side leans towards the tunnel surface. The air entrainment of the fire plume is stronger than

that in the open. Experimental data of air entrainment through ventilated windows from Quintiere et al [16] support the trend that the extra air entrainment due to wind increases almost linearly with the air velocity through the ventilated window. The ratio of mass flow rate of the fire plume in a ventilated flow to that in the open can be expressed as [10]:

$$\frac{m_p(z)}{m_{p,o}(z)} = C_k V' \quad (7)$$

where $m_p(z)$ is the mass flow rate at a given height in a ventilated flow, $m_{p,o}(z)$ is the mass flow rate at a given height in the open, and C_k is a coefficient.

Raj et al. studied the effect of wind on LNG pool fires and proposed a formula to estimate the flame angle due to wind, for methane which can be expressed as [16][17]:

$$\sin \theta = \begin{cases} 1, & V' \leq 0.19 \\ (5.26V')^{-1/2}, & V' > 0.19 \end{cases} \quad (8)$$

The flame angle θ in Equation (8) is defined as the angle between the flame axis and the horizontal surface. It is shown that when the ventilation velocity is small, i.e. when $V' \leq 0.19$, the flame is hardly deflected and the ventilated flow has no effect on the fire plume. Consequently, the plume mass flow rate does not increase. In addition, when the ventilation velocity is high ($V' > 0.19$), the flame deflects and the ventilated flow induces extra air entrainment into the fire plume in a ventilated flow, so that the plume mass flow rate increases with the ventilation velocity. Consequently, the boundary condition for this transition can be expressed as:

$$V' = 0.19 \quad (9)$$

Note that the ratio of the mass flow rate of the fire plume in a ventilated flow to that in the open, as defined in Equation (7), should be equal to 1 under this condition, both when the dimensionless ventilation velocity is lower than 0.19 ($V' \leq 0.19$) and when the dimensionless ventilation velocity is greater than 0.19 ($V' > 0.19$). Consequently, the coefficient C_k can be given as:

$$C_k = \begin{cases} 1/V', & V' \leq 0.19 \\ 5.26, & V' > 0.19 \end{cases} \quad (10)$$

Substituting Equation (6) and Equation (10) into Equation (7) yields:

$$m_p(z) = \begin{cases} 0.071Q_c^{1/3} z^{5/3}, & V' \leq 0.19 \\ 0.3735Q_c^{1/3} z^{5/3} V', & V' > 0.19 \end{cases} \quad (11)$$

2.3 Formulas for standardized time-temperature curves

In the following, a short summary of the mathematical expressions for various standardized time-temperature curves is given. These expressions will be used later in the

report to explore the relationship between the standardized curves and examples from different tunnel scenarios.

One standard curve used when testing the temperature exposure is the cellulose curve defined in several standards, e.g. ISO 834 [2]. This curve applies to materials found in typical buildings and is expressed as:

$$\Delta T(t) = 345 \lg(8t+1) \quad (12)$$

where t is the time (min).

ISO 834 curve has been used for many years, also for tunnels, but it is clear that this curve does not represent all materials, e.g. petrol, chemicals, etc., and therefore a special curve, the hydrocarbon curve (the HC curve), which was developed in the 1970s for use in the petrochemical and off-shore industries, has been applied to tunnels [3] in recent years. The main difference between these two curves is that the HC curve exhibits a much faster fire development and consequently is associated with a faster temperature increase than the standard ISO 834 fire curve and has traditionally been seen to be more relevant for a petroleum fire. The Hydrocarbon Curve (HC) can be expressed as follows:

$$\Delta T(t) = 1080[1 - 0.325 \exp(-0.167t) - 0.675 \exp(-2.5t)] \quad (13)$$

where t is the time (min).

Alternative (specific) temperature curves have been developed in some countries to simulate other hydrocarbon fires in tunnels. Examples of such curves are the Rijkswaterstaat Tunnel Curve (RWS curve) in the Netherlands [4] and the RABT/ZTV Curve in Germany [5].

PIARC recommends the use of the ISO 834 curve (60 min) for cars and vans and the RWS curve or the modified HC curve (HCM, 120 min) [6] for trucks and tankers. These recommendations are agreed by the International Tunnelling Association (ITA).

2.4 Maximum excess gas temperature beneath ceiling

2.4.1 Small fire

We assume that the velocity and temperature profiles are of similar shape, independent of the height. Further, we assume that these profiles are what are known as top-hat profiles, so that the velocity and temperature are constant over the horizontal section at a given height. This is a normal assumption for axisymmetric fire plumes in the open [13].

In addition, the radiative energy is typically in the range of 20 to 40% of the total energy released from many common fuel sources [13]. This means that 70 % of the total heat release rate is a reasonable value to be used as a convective heat release rate. The average excess temperature of the fire plume above ambient at a given height can be expressed as:

$$\Delta T(z) = \frac{Q_c}{m_p(z)c_p} = \frac{(1 - \chi_r)Q}{m_p(z)c_p} \quad (14)$$

where χ_r is the fraction of convective heat release rate in total heat release rate.

According to research on plume flow in the open, the weak plume assumptions can be relaxed. In addition, note that the maximum temperature of the fire plume at the tunnel height is the maximum temperature of the buoyancy-driven smoke flow beneath the tunnel ceiling. This means that the effective tunnel height, i.e. the vertical distance between the bottom of the fire source and the tunnel ceiling, H_{ef} , is the vertical distance above the bottom of the fire source, z , under this condition., see Figure 3.

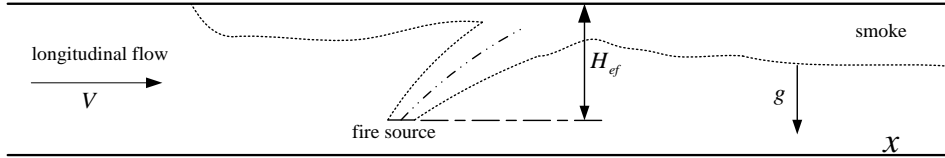


Figure 3 Definition of the effective tunnel ceiling height, H_{ef} .

Lönnermark and Ingason [18] have shown that the width of the tunnel has very little effects on the maximum ceiling temperature. They used a wide range of different tunnel widths in a model scale test series and were not able to see any effects of the tunnel width. Therefore, the width has not been included in the subsequent analysis.

The maximum gas excess temperature beneath the ceiling can therefore be expressed as:

$$\Delta T_{\max} = C_T \Delta T(H_{ef}) \quad (15)$$

Substituting Equation (11) and Equation (14) into Equation (15) gives

$$\Delta T_{\max} = \begin{cases} 14.1 C_T (1 - \chi_r)^{2/3} \frac{Q^{2/3}}{H_{ef}^{5/3}}, & V' \leq 0.19 \\ \frac{2.68 C_T (1 - \chi_r)^{2/3} g^{1/3}}{(\rho_o c_p T_o)^{1/3}} \frac{Q}{V b_{fo}^{1/3} H_{ef}^{5/3}}, & V' > 0.19 \end{cases} \quad (16)$$

From Equation (16), it is seen that the maximum gas excess temperature beneath the tunnel ceiling can be categorized into two regions. When the dimensionless ventilation velocity, V' , is lower than 0.19 (Region I), the plume mass flow rate in a ventilated tunnel is almost equal to that in the open, and so the maximum gas excess temperature is the same as that expected in the open, independent of the ventilation velocity. Further, the maximum gas excess temperature varies as a two-thirds power law of the heat release rate. This phenomenon occurs at a high heat release rate or at a very low ventilation velocity.

When the dimensionless ventilation velocity, V' , is greater than 0.19 (Region II), the mass flow rate of the fire plume in a ventilated tunnel increases linearly with the ventilation velocity and decreases slightly with the heat release rate. As a consequence, the maximum gas excess temperature decreases linearly with the ventilation velocity and increases linearly with the heat release rate, as shown in Equation (16). In addition, the maximum excess gas temperature varies as a $-5/3$ power law of the effective tunnel height in both regions.

In other words, the maximum excess gas temperature beneath the tunnel ceiling increases linearly with the heat release rate and decreases linearly with the longitudinal ventilation velocity when the dimensionless ventilation velocity, V' , exceeds 0.19 (Region II). When the dimensionless ventilation velocity is lower than 0.19 (Region I), the maximum gas excess temperature beneath the tunnel ceiling varies as the two-thirds power of the heat release rate, independently of the longitudinal ventilation velocity. In both regions, the maximum gas excess temperature varies as a $-5/3$ power law of the effective tunnel height.

Equation (16) is obtained based on the assumption that the flow profile and the gas temperature profile across the section of the fire plume at any height follows a top-hat profile, and that the continuous combustion zone is lower than the tunnel height. This implies that the plume gas temperature is constant across any section of the plume. In practice, at any given height the center line gas temperature of the fire plume is higher than the average gas temperature. The coefficient, C_T , defined in Equation (15) will be modified by experimental data.

In the previous study concerning the maximum excess gas temperature beneath the tunnel ceiling by Li et al. [10], the following equation was proposed:

$$\Delta T_{\max} = \begin{cases} 17.5 \frac{Q^{2/3}}{H_{ef}^{5/3}}, & V' \leq 0.19 \\ \frac{Q}{Vb_{fo}^{1/3} H_{ef}^{5/3}}, & V' > 0.19 \end{cases} \quad (17)$$

Correlation coefficients of 0.981 and 0.982 were found for the correlations, respectively. Comparing Equation (16) and Equation (17) indicates that coefficient C_T is equal to 1.59 for the dimensionless ventilation velocity lower than 0.19 and 1.56 for higher ventilation velocity.

2.4.2 Large fire

The above correlations are not valid when the flame volume becomes very large. For a very large fire in the tunnel, the flame impinges on the tunnel ceiling, and the continuous flame volume (combustion zone) crawls along the tunnel ceiling. Therefore the maximum temperature beneath the ceiling should be the flame temperature. In such cases, the mass flow rate of the fire plume is difficult to estimate and Equation (14) collapses. Therefore the prediction of temperature of a large fire plume in a ventilated flow appears to be impossible to derive theoretically.

However, we can assume that Equation (17) should still be fulfilled before the part of the flame volume representing the combustion zone impinges on the tunnel ceiling (strong plume theory). After that the maximum temperature beneath the ceiling is represented the flame temperature. This means that in such cases the maximum temperature beneath the ceiling should be a constant, based on a vast majority of research on the flame temperature, such as McCaffrey's fire plume theory [19]. Kurioka et al [8] referred to the maximum gas temperature beneath the ceiling as 800 °C, however, gas temperatures over 1000 °C, up to 1365 °C in the Runehamar full-scale tests [20] and 1370 °C in the Memorial full-scale tests [21].

The reason why the maximum temperature beneath the tunnel ceiling is so high is that the scenario is different in an open fire or an enclosure fire. In an open fire, the flame and hot gases radiate to the surroundings, approximately without heat feedback from the

surroundings. In an enclosure fire the heat feedback from the surrounding roof and walls is normally limited due to the large space and the possible highest heat release rate is directly related to the openings. However, for a large fire in the tunnel, the heat feedback plays an important role in the heat balance between flames and hot gases, and the forced ventilation enhances the combustion. That is why a tunnel fire is normally fuel controlled in a well ventilated tunnel. As a consequence, the temperature of the flame and hot gases is higher than in an open fire or a building enclosure fire.

In order to show the significance of the boundary conditions at the ceiling we make a simple theoretical analysis of the heat losses. A simple energy balance of hot gas in the control volume, as shown in Figure 4, can be carried out. The control volume lies beneath the tunnel ceiling and includes the whole flame volume beneath the ceiling. The mass of the control volume is M_p , and its temperature is the maximum temperature beneath the tunnel ceiling, T_{max} . It is assumed that the heat radiation from other parts of the flames and hot gases to the control volume is equal to that from the control volume to the surrounding walls.

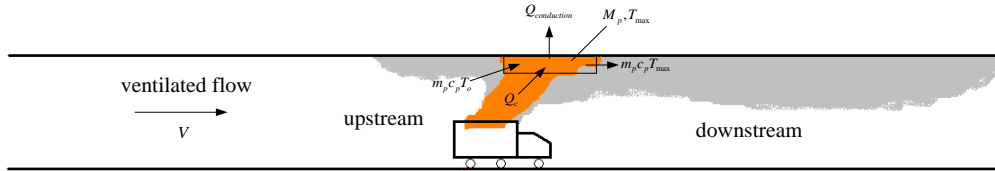


Figure 4 A diagram of heat balance of the control volume below the ceiling.

The simplified energy equation for the fire plume beneath the tunnel ceiling can be expressed as:

$$M_p c_p \frac{dT_{max}}{dt} = -m_p (T_{max} - T_o) + Q_c - Q_{conduction} \quad (18)$$

The surrounding tunnel walls absorb heat by convection and radiation, but ultimately the heat loss occurs by conduction to the surrounding wall. Assuming that the temperature of the surface is the same as the neighboring gas temperature, the heat conduction can be expressed as:

$$q''_{conduction} = Q_{conduction} / A = \sqrt{\frac{k \rho c_s}{\pi t}} (T_g - T_w) \quad (19)$$

where T_g is the gas temperature, T_w is the inner wall temperature, and k, ρ, c_s are the heat conductivity, density, and heat capacity of the material in tunnel wall. This equation is obtained based on the assumption that temperature on the boundary surface is equal to the gas temperature.

The total heat transfer coefficient, h_k , can therefore be expressed as:

$$h_k = \sqrt{\frac{k \rho c_s}{\pi t}} \quad (20)$$

The heat loss by conduction is related to the thermal properties of the tunnel wall, the gas temperature and the duration time.

The thermal penetration time, t_p , is defined as:

$$t_p = \frac{\delta^2}{4a} \quad (21)$$

where a is thermal diffusivity, given by the relation:

$$a = \frac{k}{\rho c_s} \quad (22)$$

These equations will be used later to analyze the effects of different tunnel linings on the possible heat losses to the boundaries.

Further, we know that the portion of particles in the flames and hot gases also have an influence on the maximum temperature beneath the tunnel ceiling. In a very large fire in the tunnel, the incomplete combustion in the near field of the fire site produces more particles in the hot gases. These particles hinder thermal radiation and produce a higher maximum temperature beneath the ceiling.

In conclusion, the maximum temperature beneath the ceiling in a tunnel fire is independent of the ventilation velocity if the ventilation velocity across the fire source is very low compared to the heat release rate, and the maximum temperature is just dependent on the heat release rate, however, it approaches a constant if the part of the flame volume containing the combustion zone is present at the tunnel ceiling. In other words, if $V' \leq 0.19$, the maximum excess temperature can be expressed as:

$$\Delta T_{\max} = \begin{cases} 17.5 \frac{Q^{2/3}}{H_{ef}^{5/3}}, \\ \text{Constant,} \end{cases} \quad (23)$$

If the ventilation velocity across the fire source increases, the maximum excess temperature beneath the ceiling depends on both the heat release rate and the ventilation velocity, however, it also approaches a constant if the combustion zone is present at the tunnel ceiling. How to determine which constant to use will be discussed in chapter 3. In other words, if $V' > 0.19$, the maximum excess temperature can be expressed as:

$$\Delta T_{\max} = \begin{cases} \frac{Q}{V b_{fo}^{1/3} H_{ef}^{5/3}}, \\ \text{Constant,} \end{cases} \quad (24)$$

The maximum excess temperature in the constant regions is almost a constant, but it is still dependent on some parameters, such as the thermal properties of tunnel wall and vehicles, as explained earlier. How to determine which constant should be used will be discussed in chapter 5.

Note that the parameter called radius of the fire source b_{fo} used in the equations given earlier is important. For a circular fire source, the radius of the fire source is easy to determine. For a rectangular fire source, such as a gas fire or pool fire, an equivalent circular radius of the fire source should be used based on equivalent area of fire source.

The same method is used for a wood crib fire. In such cases, a horizontal slice across the geometrical centre of the fire source can be regarded as equivalent geometry of the fire source.

It should also be noted that the height used here is not the tunnel height, but the effective tunnel height, H_{ef} , i.e. the vertical distance between the bottom of the fire source and the tunnel ceiling. This parameter is very important for the determination of the maximum excess temperature beneath the ceiling in a tunnel fire.

2.5 Position of maximum temperature beneath tunnel ceiling

The position of the maximum temperature beneath the ceiling in a ventilated tunnel fire is very important for predicting the activation of the detection system and automatic sprinkler system in a tunnel. It is also important when estimating the fire characteristics in a ventilated tunnel flow.

A drawing showing the position of maximum temperature beneath the ceiling, L_{MT} , is given in Figure 3. Here a flame angle, φ , is defined as the angle between the horizontal line and the line connected fire source centre and the position of maximum temperature. Therefore the flame angle φ is defined based on position of the maximum temperature.

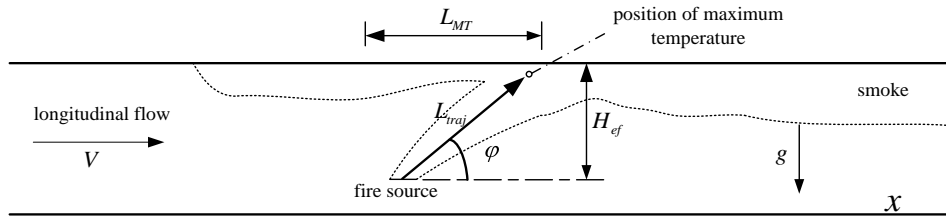


Figure 5 A diagram of the flame angle, φ , and the position of the maximum temperature, L_{MT}

2.5.1 A short review

As described previously, Raj et al. [17] propose a formula to predict the flame angle in open fires, for methane, which can be expressed as:

$$\sin \theta = \begin{cases} 1, & V' \leq 0.19 \\ (5.26V')^{-1/2}, & V' > 0.19 \end{cases} \quad (25)$$

This equation was obtained based on experimental data from fire tests conducted in the open. It should be kept in mind that the flame angle θ in Equation (25) is slightly different to the flame angle in a tunnel fire discussed here.

Kurioka et al [8] proposed an equation to calculate the position of the maximum temperature beneath the ceiling in a longitudinally ventilated tunnel fire, which is expressed as:

$$\frac{L_{traj}}{H_{ef}} Fr^{1/2} = \alpha \left[\frac{H^{3/2} Fr Q'^{(2\eta-1)/5}}{b^{1/2} A_f^{1/2}} \right]^\beta \quad (26)$$

where L_{traj} is the distance between fire source centre to the position of the maximum temperature, H is the tunnel height, and α , β and η are empirical coefficients determined from experimental data.

The Froude Number Fr is defined as:

$$Fr = \frac{V^2}{gH_{ef}} \quad (27)$$

The dimensionless heat release rate is defined as:

$$Q' = \frac{Q}{\rho_o c_p T_o g^{1/2} H_{ef}^{5/2}} \quad (28)$$

The empirical coefficients for α , β and η are listed in Table 1. The treatment by Kurioka et al. yields three regions, depending on the maximum temperature value beneath the ceiling.

Table 1 Coefficients in Equation (26).

	ΔT_{max}	η	α	β
Region 1	< 250	-1/3	0.79	0.73
Region 2	250 ~ 550K	0	0.92	0.60
Region 3	~ 550	1/2	1.02	0.56

Note that the Froude Number Fr exists in both sides of Equation (26). If experimental data is plotted using such an approach, the data fitting appears to be better than what it should be otherwise.

Equation (26) is transformed into the following to make the comparison latter more realistic:

$$\sin \varphi = \frac{H_{ef}}{L_{traj}} = \frac{1}{\alpha} Fr^{1/2} \left[\frac{H^{3/2} Fr Q'^{(2\eta-1)/5}}{b^{1/2} A_f^{1/2}} \right]^{-\beta} \quad (29)$$

2.5.2 Small fire

Experimental data of air entrainment through ventilated windows from Quintiere et al [16] support the trend that the mass flow rate of fire plume in a ventilated flow is almost equal to that in the open by use of the inclined flame path as the plume height.

The entrainment velocity of the fire plume, however, may be different. Therefore it is assumed that the mass flow rate of inclined fire plume in a ventilated tunnel can be calculated by the same method as that in the open, and the only difference is the inclined path and the entrainment velocity which can be expressed as:

$$v = \alpha' u \quad (30)$$

where v is the entrainment velocity, α' is the entrainment coefficient.

Based on the above assumption, the mass flow rate of the fire plume in a ventilated flow at a given height z , $m'_{po}(z)$, can be expressed as:

$$m'_{po}(z) = \pi \left(\frac{6}{5}\right)^2 \left(\frac{25}{48} \frac{\rho_o^2 g}{\pi c_p T_o}\right)^{1/3} \alpha'^{4/3} Q^{1/3} z^{5/3} \propto Q^{1/3} z^{5/3} \quad (31)$$

According to the former analysis, the mass flow rate in a ventilated tunnel can also be expressed as:

$$m_p(z) = \begin{cases} 0.3735 Q_c^{1/3} H_{ef}^{5/3} V', & V' > 0.19 \\ 0.071 Q_c^{1/3} H_{ef}^{5/3}, & V' \leq 0.19 \end{cases} \quad (32)$$

Equation (31) and Equation (32) should equal to each other, i.e. :

$$m'_{po}(L_{traj}) = m_p(z) \quad (33)$$

Note that when the ventilation velocity is very low, the plume is not inclined by a horizontal wind (or at least only to a very moderate degree), so the flame angle should approach 90 degree.

Thus, we can obtain:

$$\sin \varphi = \frac{H_{ef}}{L_{traj}} = \begin{cases} 1, & V' \leq 0.19 \\ k \left(\frac{gQ}{\rho_o T_o c_p V^3 b_{fo}} \right)^{1/5}, & V' > 0.19 \end{cases} \quad (34)$$

where k is a coefficient defined from experimental data.

The continuity of the equations should be fulfilled. Therefore Equation (34) can be transformed into:

$$\sin \varphi = \frac{H_{ef}}{L_{traj}} = \begin{cases} 1, & V' \leq 0.19 \\ (5.26V')^{-3/5}, & V' > 0.19 \end{cases} \quad (35)$$

Note that experimental data concerning air entrainment from Quintiere et al [16] support the trend that the mass flow rate of the fire plume in a ventilated flow is almost equal to that in the open by use of the inclined flame path as the plume height. This means that the entrainment velocity of the fire plume can be considered as the same. Under such conditions we can also obtain Equation (35). Comparing this with Raj et al.'s formulae for the flame angle due to wind shows that the equations is almost the same, and the only difference is the power coefficient of -0.6 for Equation (35) and -0.5 for Raj et al.'s formulae.

The position of the maximum temperature beneath tunnel ceiling, L_{MT} , can be expressed as (see figure 6):

$$L_{MT} = H_{ef} \cot(\arcsin \theta) \quad (36)$$

where H_{ef} is the effective height, i.e. the vertical distance between the tunnel ceiling and the bottom of the fire source.

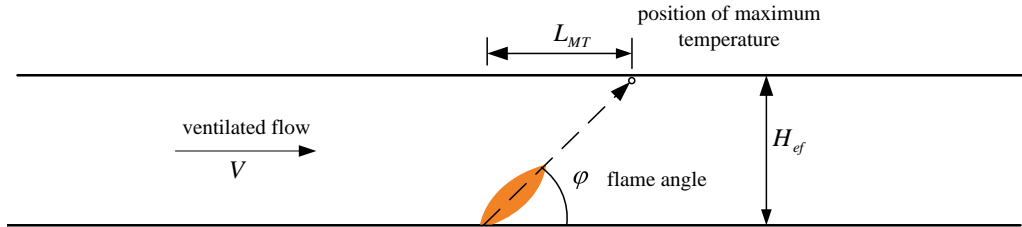


Figure 6 A definition of the flame angle and position of the maximum temperature in a small tunnel fire.

2.5.3 Large fire

It should be pointed out here that the scenario is slightly different when the flames become very large. Figure 7 shows the flame angle and position of the maximum temperature in a large tunnel fire. The flame angle is relatively easy to determine in an open fire. For a large fire in a tunnel, the flame impinges on the ceiling and crawls along the tunnel ceiling. However, the impingement point should also represent the point of maximum temperature beneath the ceiling. According to previous work on the flame length and the distribution of ceiling temperature [22], the temperature beneath the tunnel ceiling in a certain range close to the fire, where the continuous flame region lies, is almost a constant. In other words, the maximum temperature beneath the tunnel ceiling in a large fire exists in a certain range close to the fire, not only a single point. Based on the equations for flame length and distribution of ceiling temperature in a tunnel fire, this range, defined as starting at the fire source centre to the virtual origin, can be determined. Here the projection point is defined as the position of the maximum temperature beneath the tunnel ceiling, see Figure 7. Based on this definition, Equation (35) should still be valid.

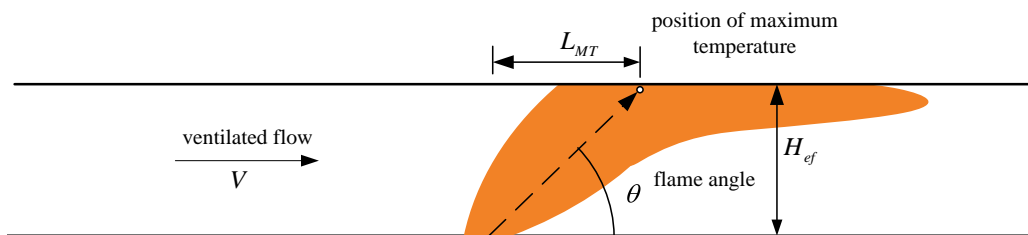


Figure 7 A diagram of flame angle for a large fire in a tunnel.

Based on the above analysis of the flame angle, one can conclude that it is dependent on the ratio of the ventilation velocity and the dimensionless plume velocity for a small fire in a tunnel.

If the ventilation velocity across the fire is low, there should be some smoke backflow upstream of the fire, which is called back-layering. According to a previous study of smoke control in longitudinally ventilated tunnels [23], the dimensionless back-layering length, L_b^* , can be expressed as:

$$L_b^* = \frac{L_b}{H} = \begin{cases} 18.5 \ln(0.81 \text{Ri}'^{1/3}) & Q^* \leq 0.15 \\ 18.5 \ln(0.43/V^*) & Q^* > 0.15 \end{cases} \quad (37)$$

The modified Richardson Number, Ri' , dimensionless longitudinal velocity, V^* , and dimensionless heat release rate, Q^* , in Equation (37) are defined respectively as:

$$\text{Ri}' = \frac{gQ}{\rho_o c_p T_o V_o^3 H} \quad V^* = \frac{V}{\sqrt{gH}} \quad Q^* = \frac{Q}{\rho_o c_p T_o g^{1/2} H^{5/2}} \quad (38)$$

It should be kept in mind that these equations don't take the geometry of the fire source into account. However, Equation (37) means, for a large fire in a tunnel, i.e. when $Q^* > 0.15$, that the back-layering length is independent of heat release rate, and only related to the ventilation velocity.

Note that the modified Richardson Number in Equation (38) can be related to the dimensionless ventilation velocity as:

$$\text{Ri}' = \frac{b_{fo}}{H} V'^{-3} \quad (39)$$

For a small fire in a tunnel, it can be seen that both the flame angle and the back-layering length are directly related to the modified Richardson Number. It can, therefore, be speculated that for a large fire in a tunnel, the flame angle is also independent of the heat release rate, in the same way that was just proved for the back-layering length. Due to the continuity of the equations in the transition point, the full expression of the flame angle is:

$$\sin \varphi = \frac{H_{ef}}{L_{traj}} = \begin{cases} 1, & V' \leq 0.19 \\ (5.26V')^{-3/5}, & V' > 0.19 \ \& \ Q^* \leq 0.15 \\ 0.25(b_{fo}V'^3/H)^{-1/5} & V' > 0.19 \ \& \ Q^* > 0.15 \end{cases} \quad (40)$$

According to Equation (40), it can be seen that the flame angle can be categorized into three zones. The flame angle is 90° if the dimensionless ventilation velocity is lower than 0.19. If $V' > 0.19$, the flame angle varies as $-3/5$ power law of V' when $Q^* \leq 0.15$, and it is independent of heat release rate when $Q^* > 0.15$.

2.5.4 Critical flame angle

As the ventilation velocity increases, the back-layering length will decrease accordingly. As the ventilation velocity is equal to the critical velocity, the back-layering just disappears, which is equal to the critical condition. The flame angle at this critical condition is defined here as the ‘‘critical flame angle’’ in a ventilated tunnel fire. According to the previous work [23], the critical velocity in a ventilated tunnel fire can be expressed as:

$$V_c^* = \begin{cases} 0.81Q^{*1/3}, & Q^* \leq 0.15 \\ 0.43, & Q^* > 0.15 \end{cases} \quad (41)$$

Note that the critical modified Richardson Number can be expressed as:

$$Ri'_c = \frac{b_{fo}}{H} V_c^{-3} \quad (42)$$

Comparing Equation (40) and Equation (41) shows that Equation (42) should still be valid even at a high heat release rate. Combining these equations, the critical flame angle can be simply expressed as:

$$\sin \varphi_c = k_c \left(\frac{b_{fo}}{H} \right)^{-1/5} \quad (43)$$

where k_c is a coefficient, 0.42.

This means that for a given tunnel and fire source, the critical flame angle is always of the same value in a tunnel fire. Consequently, the position of the maximum temperature beneath the tunnel ceiling remains the same. This means that there is a critical position of the maximum temperature corresponding to the critical condition, i.e. the back-layering just disappears.

3 Discussion of results

In Appendix A and B, a summary of data from model scale tunnel fire tests and large scale tunnel fire tests is presented. In Appendix A, a description of and tabulated data from numerous model scale tests carried out at SP is given. In Appendix B, corresponding information for large scale tests carried out worldwide is given. The summary is based on original collection and analysis of data carried out by Ingason [33]. The data from these tests has been used to investigate the validity of the theoretical formulae derived in Chapter 2. Based on the data and analysis, theoretical model for predicting the maximum temperature is proposed. The model is compared with transient test results from model scale tunnel tests carried out at SP and the Runehamar tunnel fire tests carried out by a Consortium led by SP in Norway. The position of the maximum temperature was also analyzed. The equation obtained by theoretical analysis was compared with equations in other literatures.

3.1 Maximum excess temperature beneath tunnel ceiling

According to the theoretical analysis, the maximum gas excess temperature below the tunnel ceiling increases linearly with the heat release rate and decreases linearly with the longitudinal ventilation velocity when the dimensionless ventilation velocity, V' , is greater than 0.19 (Region II). When the dimensionless ventilation velocity is lower than 0.19 (Region I), the maximum excess gas temperature below the tunnel ceiling varies as two-third power of the heat release rate, independent of the longitudinal ventilation velocity. In both regions, if the heat release rate increases, the maximum excess temperature approaches a constant value. In the following, all the data that has been correlated using Equation (23) and Equation (24) are presented.

3.1.1 Model scale tests

In Figure 8 and 9, the data for the maximum gas excess temperature below the tunnel ceiling from all the model scale tests presented in Appendix A, when the dimensionless ventilation velocity is lower than 0.19 (Figure 8) or greater than 0.19 (Figure 9), is shown. It can be seen that the maximum excess gas temperature can be divided into two clearly defined regions: a growth region and a constant region. In the growth region, the maximum excess temperature increases linearly with the parameter obtained by theoretical analysis. In the constant regions, the maximum excess gas temperature is relatively constant, ranging from 950 °C to 1150 °C. In these two figures, the fit of the maximum excess gas temperature in the constant regions is best represented by a temperature of 1000 °C. This fit agrees well with the experimental data for all the model scale tests presented in this report.

The coefficient C_T from Equation (16) is found to be equal to 1.57 when the dimensionless ventilation velocity is less than 0.19 (Region I) and 1.56 for higher ventilation velocity (Region II). This verifies the selection of 0.19 as the transition point, and also means that the condition for this transition that the dimensionless ventilation velocity approaches 0.19 is appropriate to estimate the fire plume properties in fires in longitudinally ventilated tunnels. More information can be found in reference [10].

In practice, the ventilation velocity does influence the maximum gas temperature if the dimensionless ventilation velocity is lower than 0.19, but the effect is so small that it can

be neglected. Further, experimental data show that the position of maximum gas temperature below the ceiling does not move under such conditions.

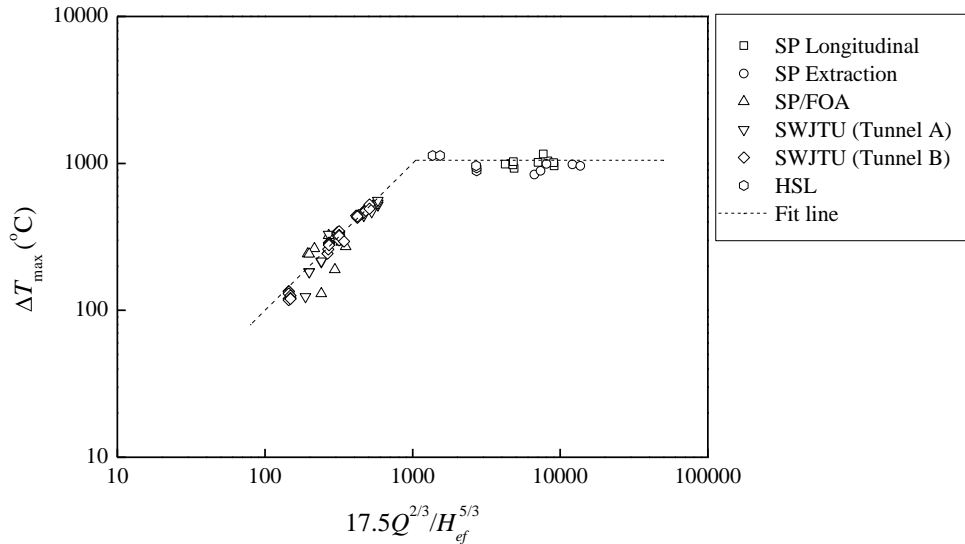


Figure 8 The maximum excess temperature beneath the tunnel ceiling in model scale tests (Region I, $V' \leq 0.19$).

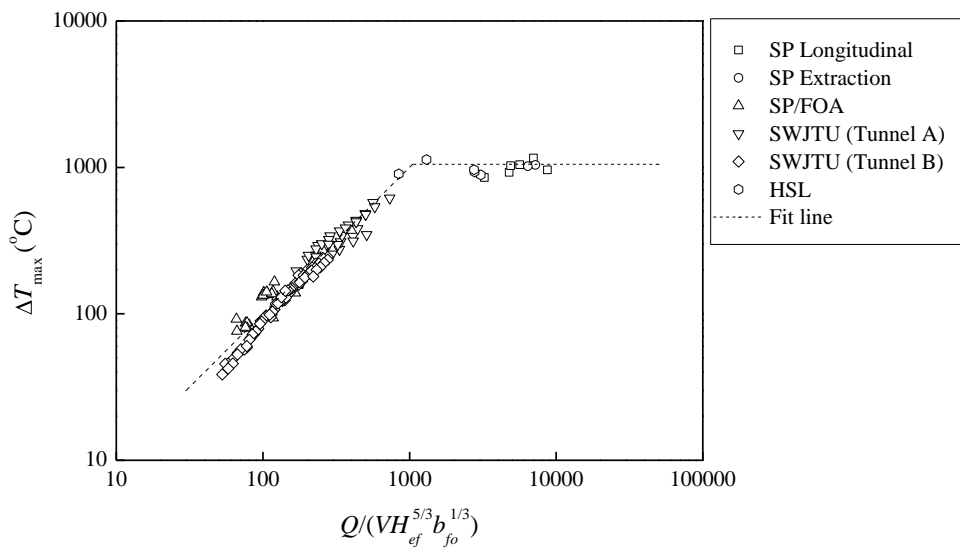


Figure 9 The maximum excess temperature beneath the tunnel ceiling in model scale tests (Region II, $V' > 0.19$).

3.1.2 Large scale tests

According to theoretical analysis, the ventilation velocity across the fire is expected to have a great influence on the maximum excess temperature beneath the tunnel ceiling and affect many other important tunnel fire characteristic properties. In a complicated tunnel ventilation system, if the exact ventilation velocity is known, the maximum excess temperature beneath the ceiling can be predicted well. However, for a transverse ventilation system, or semi-transverse ventilation system, the ventilation velocity across

the fire is usually not known. What we know is that the ventilation velocity across the fire in such cases is usually not high, and would therefore fulfill the condition $V' < 0.19$ in most cases. This means that the maximum excess temperature beneath the ceiling can be estimated by Equation (23). Large amounts of data from Memorial tunnel tests with fully-transverse ventilation system, semi-transverse ventilation system and others correlate well with Equation (23) and therefore support this hypothesis.

According to the theoretical analysis, the criteria to categorize data into Region I ($V' \leq 0.19$) and Region II ($V' > 0.19$) is the value of the dimensionless ventilation velocity, V' . Given that the ventilation velocity across the fire source is normally low for natural ventilation systems, transverse ventilation systems, semi-transverse ventilation systems and point extraction systems we propose to categorize those systems into Region I ($V' \leq 0.19$), which means that an air flow with a very low velocity passes the fire source. This results in a limited effect of ventilation on the flame and gas temperature. It may not be correct in all cases, but in most cases this should be a sufficient design criterion.

Figure 10 and 11 show data for the maximum excess gas temperature below the tunnel ceiling from all the large scale tests depicted in Appendix B, when the dimensionless ventilation velocity is less than 0.19 or greater than 0.19, respectively. It is shown that the maximum excess gas temperature can be simply divided into two regions: a growth region and a constant region, in the same manner as the data from model scale tests. The main difference from the large scale tests data is that the maximum excess temperatures apparently lie at higher levels. The measured maximum excess gas temperature beneath tunnel ceiling in the constant regions ranges from 1150 °C to 1350 °C. In Figure 10 and 11, the fit of maximum excess gas temperature in the constant region is best represented by an excess gas temperature of 1250 °C.

It is also shown in Figure 10 and 11 that the fit for the growing region complies well with the experimental data from all the large scale tests presented in this report. However, in Figure 10 some data from the Eureka and Memorial tests show a scattering trend. The reason for this will be discussed later.

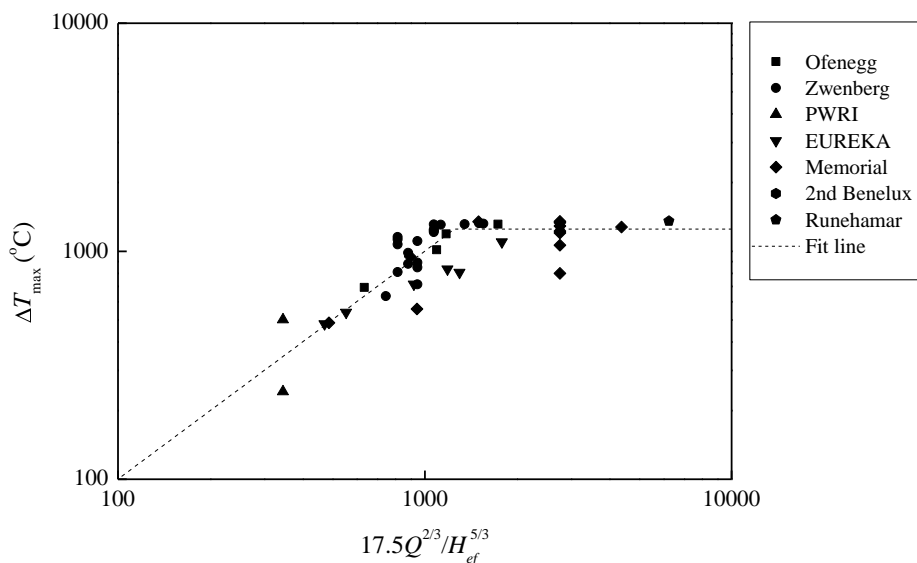


Figure 10 The maximum excess temperature beneath the tunnel ceiling in large scale tests (Region I, $V' \leq 0.19$).

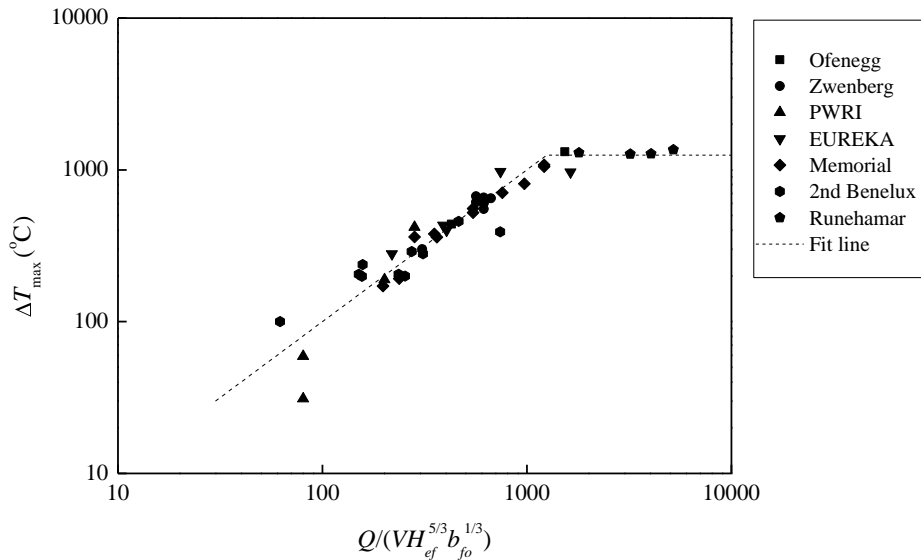


Figure 11 The maximum excess temperature beneath the tunnel ceiling in large scale tests (Region II, $V' > 0.19$).

3.1.3 Analysis of the constant regions

The above analysis shows some differences between the data for the maximum excess temperature from the large scale tests compared to that from the model scale tests. The large scale data apparently lies at higher levels than the data from the model scale tests. In addition, data from some large scale tests show a scattering trend that needs to be analysed further.

Based on previous discussion and the theoretical analysis of the plume flow and thermal response of the tunnel structure, we conclude that those parameters that may have an influence on the measured maximum temperature are most likely governed by:

- (1) the height between the bottom of the fuel and the tunnel ceiling
- (2) the heat release rate of the fuel
- (3) the ventilation type and tunnel flow rate
- (4) the combustion efficiency of the fuel in relation to type of tunnel ventilation and geometry of the fuel
- (5) the thermal properties of the surrounding tunnel walls
- (6) the thermal properties, body type and interior of the burning vehicles
- (7) the geometry of the fuel and its porosity
- (8) the duration of the high gas temperature, i.e. the high heat release rate and low ventilation velocity
- (9) the leakage rate of water from surrounding tunnel walls
- (10) the position and numbers of the thermocouples used in the near field of the fire
- (11) incorrect information concerning the position of thermocouples, such as too large an interval among thermocouples in the near field of the fire
- (12) instrument error or other experimental error

The variety of different boundary conditions makes it difficult to pinpoint one parameter that governs the maximum gas temperature but the parameters listed above are listed in order of importance.

In most of large scale tests, the tunnel structure in the vicinity of the fire source is protected from heat damage or collapse by some lining material. These materials may be

fibre insulating board, Promatect board or some other type of insulation. The properties of wall materials commonly used in a tunnel fire are listed in Table 2. Normally the innermost material of tunnel structures plays a very important role in the heat conduction. In the Runehamar tests, Promatect boards were used to protect the tunnel walls in a range of 12.5 m upstream to 53.5 m downstream of the fire. The tunnel used in the EUREKA tests was a rock tunnel, protected by a special spray concrete during the tests. The roof of the Memorial tunnel in the vicinity of the fire source was probably insulated in some way. In order to demonstrate the effects of different types of tunnel surface materials, the results of a calculation using Equation (21), is shown in Table 2.

Table 2 Thermal properties of tunnel walls and vehicles inside commonly used in tunnel fire tests.

Material		k	ρ	c_p	t_p^*	Relevant tests
		W/m ² K	kg/m ³	J/kg K	Min	
tunnel wall	Promatect	0.19	870	1130	3.59	Runehamar
	Concrete	1.10	2100	880	1.17	Memorial side walls
	Fiber insulating board	0.04	2090	229	8.11	
	Rock	2.83	2640	820	0.53	EUREKA
Vehicle	Steel	54	7833	465	0.05	EUREKA
	Aluminum	204	2707	896	0.01	EUREKA

* thermal penetration time of 0.1 m depth based on Equation (21).

Figure 12 shows the effect of thermal properties of the surrounding walls on the thermal penetration time. It is shown that the heat transfer coefficient h_k decreases with time, which in turn means that the heat transfer decreases with time. It is also shown that the heat transfer coefficient of rock is much higher than for other materials. The sequence, from high to low, is as follows: rock, concrete, Promatect, and fibre insulating board. If we assume that the flame temperature is 1000 °C, the vertical axis represents the heat flux per square meter (kW/m²). A larger heat transfer coefficient, h_k , means a larger heat loss to the surrounding walls in a tunnel fire.

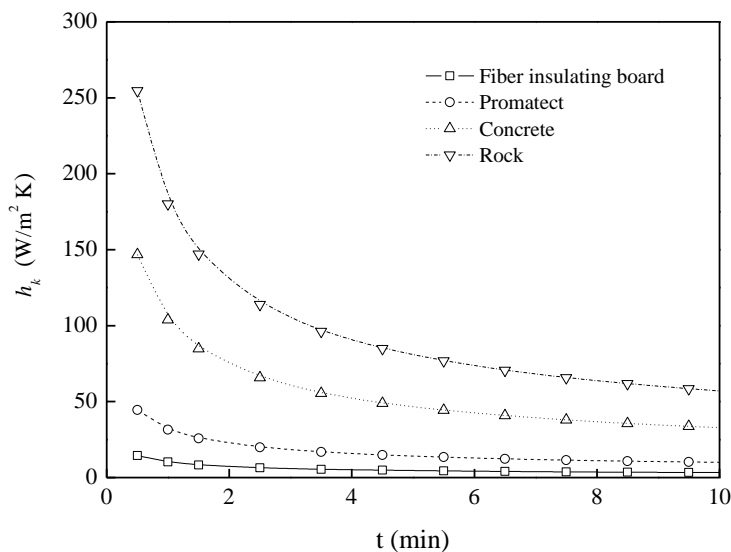


Figure 12 The effect of thermal properties of the surrounding walls.

Figure 13 and 14 present data for the maximum gas excess temperature below the tunnel ceiling from all the model scale tests and large scale tests depicted previously, when the dimensionless ventilation velocity is less than 0.19 or greater than 0.19, respectively.

Clearly, the maximum excess gas temperature beneath the tunnel ceiling lies mainly in the range of 1150 °C to 1350 °C for large scale tests and 950 °C to 1150 °C for model scale tests. The reasons for this difference can be summarized as follows:

- (1) In the model scale tests, it is not possible to preserve all the dimensionless terms derived by scaling theory.
- (2) The model tunnel wall is not scaled very well as the thickness and the thermal properties of the wall material (Promatect) enhanced the heat losses relative to the large scale. This means that relatively higher heat loss results from the thin model tunnel walls compared to large scale tests. This viewpoint is supported by an analysis of the distribution of temperature along the tunnel.
- (3) Some other reasons, such as the glaze windows installed in one side of the model tunnel in series of SP tests and FOA/SP tests, may also increase the heat loss in the near field and far field of the fire site.

It is also shown in Figures 13 and 14 that some data from the EUREKA and Memorial tunnel fire tests tends to exhibit greater scattering trend rather than a clear systematic and logical trend related to some physical parameters.

A series of data from Memorial tunnel fire tests, which forms a vertical line in Figure 13, represents data from tests with a nominal heat release rate of 50MW and a ceiling height of 4.4 m. The true ventilation velocity across the fire source is difficult to estimate due to the complexity of the ventilation system. For example in a two-zone partial transverse ventilation system, the velocity across the fire source is normally very low. Therefore, all the data involving natural ventilation systems, transverse ventilation systems, semi-transverse ventilation systems and point extraction systems were categorized into Region I ($V' \leq 0.19$). This is an attempt from the author's side to handle these uncertain data. In most cases it should succeed, however, in some special cases, it may not work. This may explain why some data of the maximum excess gas temperature are slightly lower than other data.

The maximum gas temperature from the EUREKA tests mainly ranged from 950 °C to 1150 °C. This is considerably lower than that obtained from other large scale tests. There are many possible explanations for this trend. Firstly, the majority of this data corresponds to vehicle fires, which means that the combustible materials are all burning inside the vehicle, in particular inside vehicle bodies made of steel. This means that the area of heat losses increases. Much of the energy released by the fire is thereby absorbed by the interior material and the body of the vehicle. The radiation from the flame core to the top-level flame and gas also is therefore correspondingly lower. Secondly, lots of water leaked out of the surrounding rock walls in these tests, although not close to the fire where the tunnel was protected by 50 mm thick spray concrete along a 75 m distance. The relative humidity in the tunnel prior to and after the fire tests exceeded 80% to 95 %. During the tests, the water permanently dripped and flowed from cracks in the tunnel rocks, so that the relative humidity is assumed to be around 100 % for the cooling gases further away from the fire source. Thirdly, the water inside the rock may increase the heat conduction. Finally, as discussed previously, the heat transfer of rock is much higher than other non-metal tunnel walls. Nevertheless, all these parameters and measures influence

the maximum temperature beneath the tunnel ceiling.

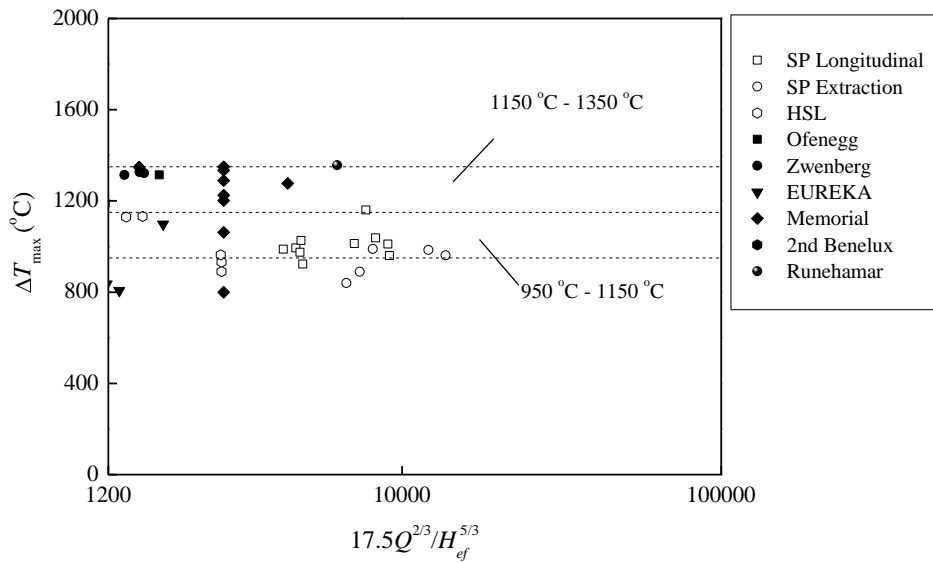


Figure 13 The maximum excess temperature beneath the tunnel ceiling in the constant region in large scale tests (Region I, $V' \leq 0.19$).

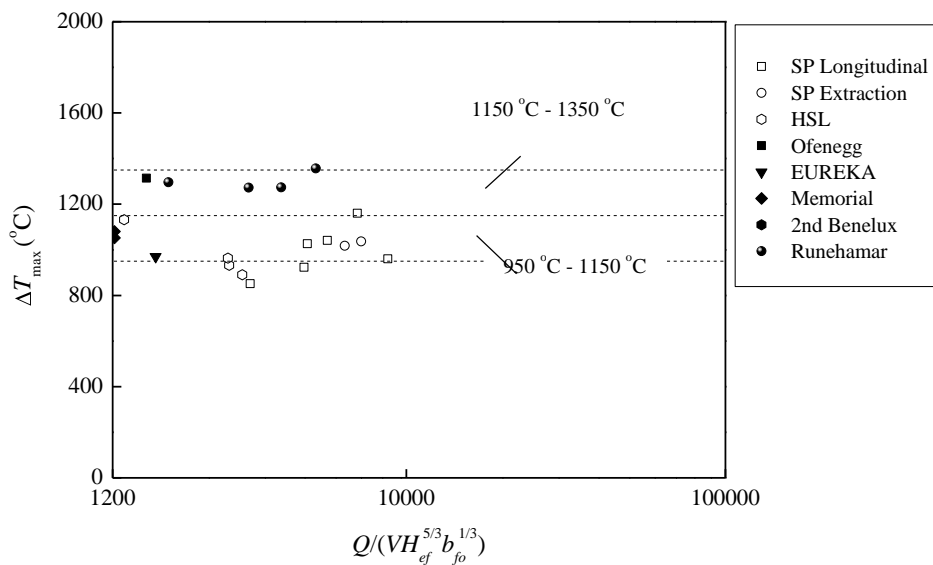


Figure 14 The maximum excess temperature beneath the tunnel ceiling in the constant region in large scale tests (Region II, $V' > 0.19$).

Note that all the excess temperature data in the range of 1150 °C to 1350 °C correspond to tests with open liquid pool fires or fires consisting of solid materials located on platforms or inside vehicles with a combustible roof. Further, note that the adiabatic gas temperature is much higher than the measured temperature, or about 2194 °C for propane [24]. Due to the heat losses discussed above it is concluded that the measured excess gas temperatures will be in the range of 1000 – 1350 °C. Note that the RWS curve yields a

maximum gas temperature of 1350 °C including the ambient temperature. This should not be confused with the excess gas temperature of 1350 °C obtained in our study.

At this stage we find it very difficult to theoretically determine the level of the constant maximum gas temperatures. The governing parameters are not very well identified and controlled, but in order to give some indications of what temperatures to expect under different conditions we propose a more empirical approach. We propose to use the experimentally highest obtained ceiling gas excess temperature of 1350 °C.

3.1.4 Formulae for maximum excess temperature

Figure 15 and 16 show all the data of the maximum temperature beneath the tunnel ceiling from the model scale tests and large scale tests given in Appendix A and B. It is shown that the data correlate well with the lines included in the figures.

In order to express the formula more clearly, two parameters are defined:

$$\text{DTR 1} = 17.5 \frac{Q^{2/3}}{H_{ef}^{5/3}}, \quad (44)$$

$$\text{DTR 2} = \frac{Q}{Vb_{fo}^{1/3} H_{ef}^{5/3}} \quad (45)$$

where DTR1 means Delta T in Region I and DTR2 means Delta T in Region II.

The maximum excess gas temperature beneath the ceiling in a tunnel fire can be divided into two regions and expressed as:

Region I ($V' \leq 0.19$):

$$\Delta T_{\max} = \begin{cases} \text{DTR 1}, & \text{DTR 1} < 1350 \\ 1350, & \text{DTR 1} \geq 1350 \end{cases} \quad (46)$$

Region II ($V' > 0.19$):

$$\Delta T_{\max} = \begin{cases} \text{DTR 2}, & \text{DTR 2} < 1350 \\ 1350, & \text{DTR 2} \geq 1350 \end{cases} \quad (47)$$

Note that there is one-one mapping between maximum temperature and the heat release rate in the linear regions, i.e. when DTR1 or DTR2 < 1350, or if DTR1 or DTR2 ≤ about 1150 for model scale tests. Therefore the inverse calculation based on the above equations works. The maximum temperature and the heat release rate can be transformed simply. It should be pointed out that the one-one mapping between them doesn't exist in the constant regions, i.e. DTR1 or DTR2 ≥ 1350, or if DTR1 or DTR2 ≥ about 1150 for model scale tests. However, the inverse calculation based on the above equations can still be used to estimate the heat release rate, which will become the minimum heat release rate required to obtain such a high temperature.

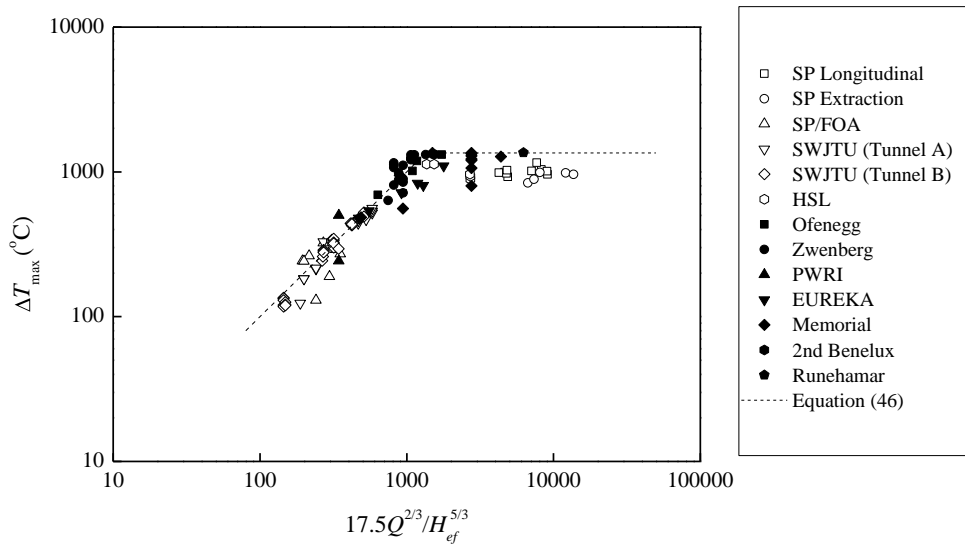


Figure 15 The maximum excess temperature beneath the tunnel ceiling (Region I, $V' \leq 0.19$).

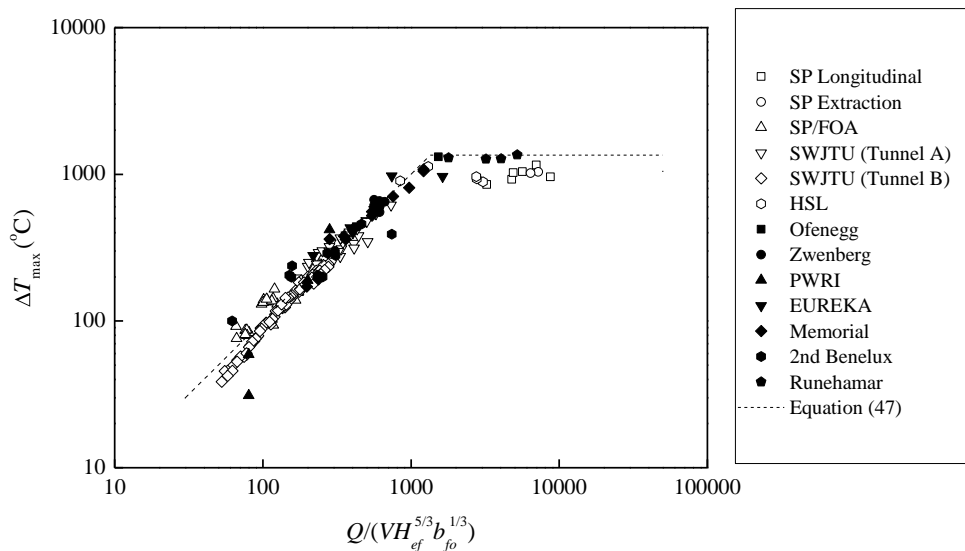


Figure 16 The maximum excess temperature beneath the tunnel ceiling (Region II, $V' > 0.19$).

3.1.5 Comparison with transient tests data

Normally in a real tunnel fire, the heat release rate varies with time. At the same time, the ventilation velocity across the fire site also varies with time, especially for a fire in a short tunnel. Therefore, the maximum excess gas temperature beneath the ceiling should also be a transient value.

In a comparable manner as in a room fire, a tunnel fire can be divided into three stages: the growth stage, the steady state stage, and the decay stage. In the growth stage, the gas

temperature increases rapidly with the heat release rate. In the steady state stage, the flame or gas temperature may still increase slowly during a certain period, but the excess gas temperature is more dependent on the decrease of the heat loss to the surrounding walls and objects. In the decay stage, the temperature of the flame and gas decreases gradually due to the decrease in the heat release rate, however, the hot surrounding walls and objects makes the decrease of temperature more slowly than expected.

All the experimental data from the model scale tests and the large scale tests presented in Appendices A and B are obtained in a quasi-steady state. For tests with gas fires and some pool fires, including the FOA/SP tests and the SWJTU model scale tests, the heat release rate is almost constant during one entire test. Therefore the results are close to steady state values. For tests with some other pool fires and solid fires, including two series of SP model scale tests and most of the large-scale tests, the heat release rate varies significantly with time. Therefore measured data of the maximum heat release rate and the maximum excess gas temperature, which are relatively steadier, were used in the analysis of the maximum excess gas temperature beneath the ceiling.

Due to the fact that the formulae proposed for the maximum temperature beneath the tunnel ceiling are obtained based on the experimental data in a quasi-steady state, the formulae are not necessarily suitable for predicting the transient maximum gas temperature beneath the ceiling in a tunnel fire. However, these two values should be close to each other. In order to investigate the difference, the calculated maximum gas temperature beneath the ceiling by the proposed formulae and the transient heat release rate was compared with the transient data of maximum gas temperature beneath the ceiling from SP longitudinal ventilation tests and Runehamar tests.

In the series of SP longitudinal ventilation tests, the heat release rate (HRR) was determined using two different measurement techniques, i.e. by measuring the fuel mass loss and by measuring the mass flow rate and gas concentrations in an exhaust duct connected to the tunnel end. For the method based on the fuel mass loss, it is assumed that the combustion is diffusion-controlled, and that the reaction of fuel and oxygen is infinitely fast. For the method of oxygen consumption, the volume fraction of CO₂ is considered. Based on the HRRs measured using these two methods, the transient maximum temperatures are calculated and compared to each other.

Data concerning the maximum excess gas temperature beneath the tunnel ceiling in Test 1, Test 6, Test 7, and Test 8 are compared to the calculated data, as shown in Figure 17, Figure 18, Figure 19 and Figure 20. In these figures, the solid and the dotted lines represent the calculated maximum excess gas temperature beneath the ceiling based on the heat release rate (HRR) measured using the fuel mass loss and oxygen consumption calorimetry, respectively. Since the dimensionless ventilation velocity is greater than 0.19 in all the tests, Equation (47) is used to calculate the transient excess gas temperature during these tests.

It is shown, in Figure 17 to Figure 20, that the calculated maximum excess gas temperature based on the HRR measured using the fuel mass loss fits the measured maximum excess gas temperature very well. The calculated maximum excess gas temperature based on method of oxygen consumption also fits the data well, except in the decay period.

Based on test results, the two methods almost obtain the same value of heat release rate in the growth period and the constant period, however, the measured heat release rates using the oxygen consumption show a clear trend of delay for a short period while in the decay stage. Interesting is that the lag in the calculated maximum temperature increases as the

heat release rate decreases in the decay stage. This in turn results in an apparently larger lag of the calculated maximum temperature based on these HRRs, which is shown in Figure 17 to Figure 20. In the growth stage and the steady state stage, the calculated maximum temperature beneath the tunnel ceiling using both methods fits the measured value well. The reason for the small lag in the growth period is mainly due to the ignition source which is placed close to the wood crib and burnt at the beginning of the tests. In the decay period, the calculated temperature should be slightly lower than the measured value due to the effect of hot tunnel walls which isn't considered in the formulae.

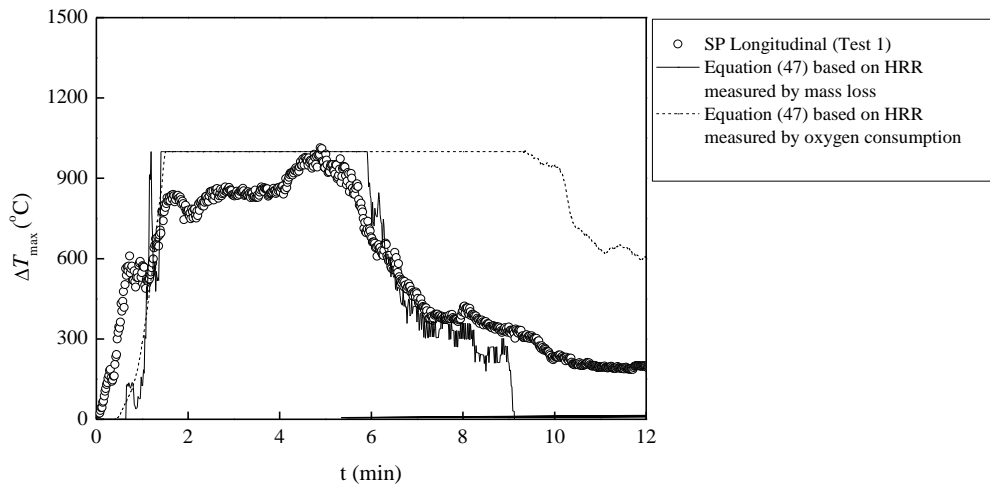


Figure 17 Comparison of calculated transient maximum temperature beneath the ceiling with data from SP longitudinal Test 1.

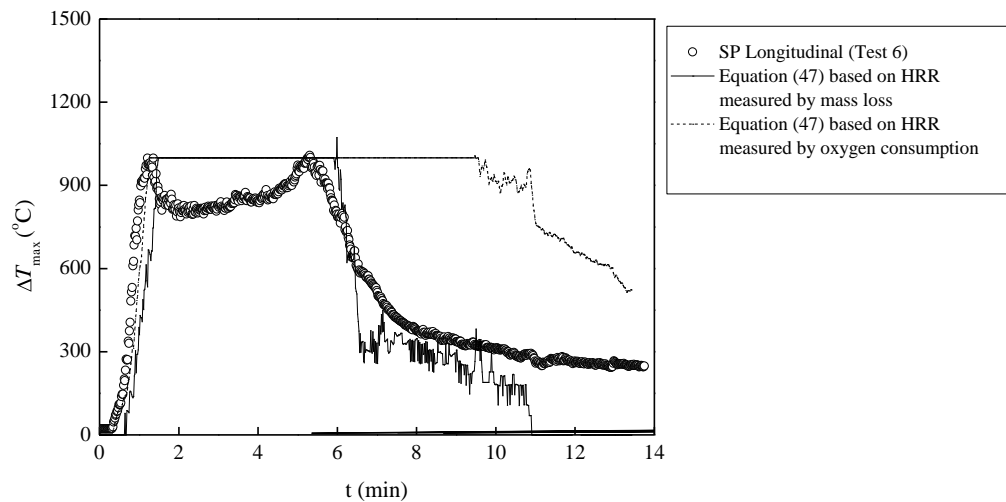


Figure 18 Comparison of calculated transient maximum temperature beneath the ceiling with data from SP longitudinal Test 6.

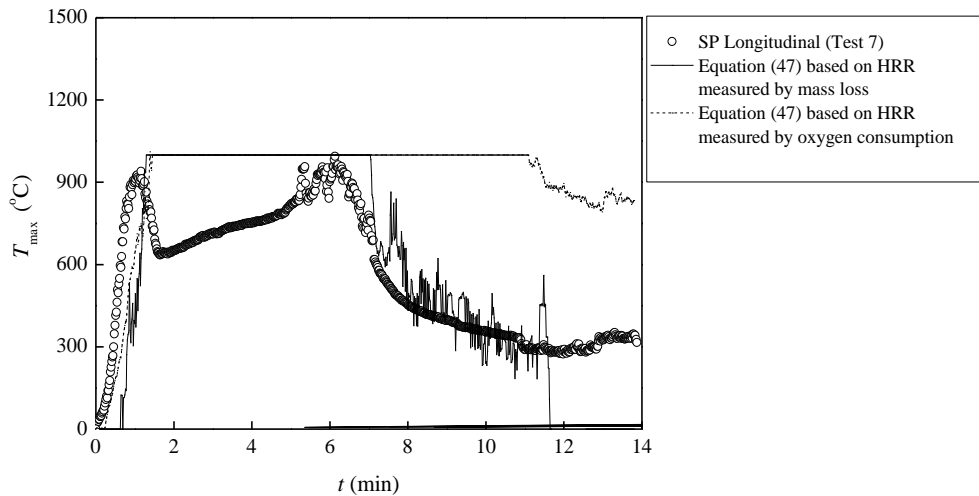


Figure 19 Comparison of calculated transient maximum temperature beneath the ceiling with data from SP longitudinal Test 7.

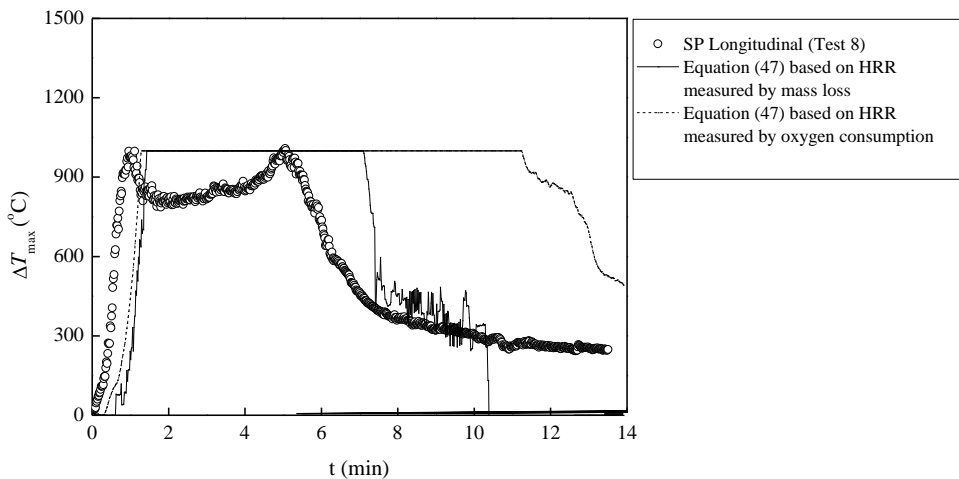


Figure 20 Comparison of calculated transient maximum temperature beneath the ceiling with data from SP longitudinal Test 8.

Data for maximum temperature beneath the tunnel ceiling in Test 1, Test 2, Test 3, and Test 4 from the Runehamar tests are compared to the calculated data respectively in Figure 21 to 24. Since the dimensionless ventilation velocity is greater than 0.19 in all the tests, Equation (47) is used to calculate the transient excess gas temperature during these tests.

It is shown in Figure 21 to 24 that the calculated maximum excess gas temperature correlate relatively well with the measured data in Test 1 and 4. The calculated values are slightly lower than the measured values in Test 3 and 4 during the fire growth periods. Similar lag that discussed above, due to using the oxygen consumption method, is also observed in all the tests, especially in Test 2, 3. Note that the maximum temperature increases much more slowly when it is over 900 °C to 1000 °C. This may mean that temperatures over 1000 °C are not closely related to the heat release rate, and may be more related to the thermal properties of the tunnel walls and vehicles close to the fire or the burning vehicle itself.

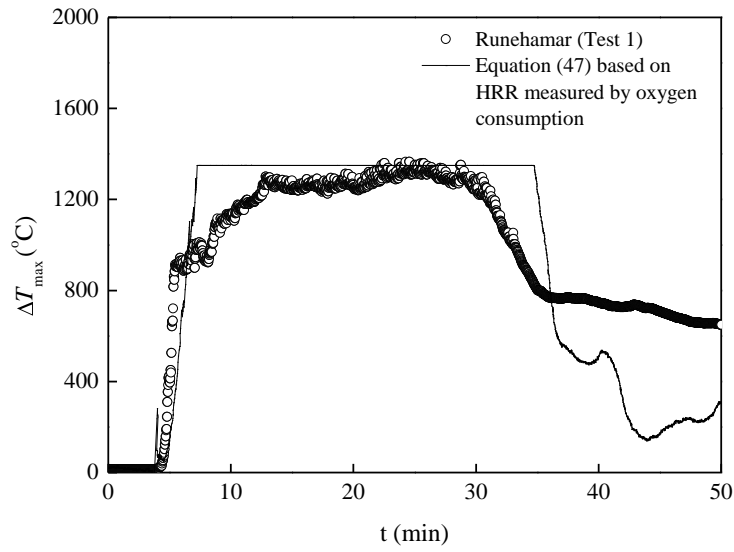


Figure 21 Comparison of calculated transient maximum temperature beneath the ceiling with data from Runehammar Test 1.

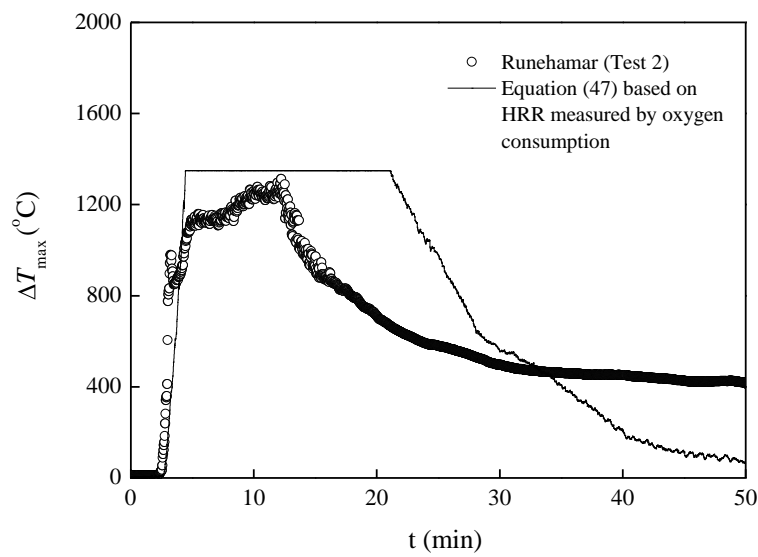


Figure 22 Comparison of calculated transient maximum temperature beneath the ceiling with data from Runehammar Test 2.

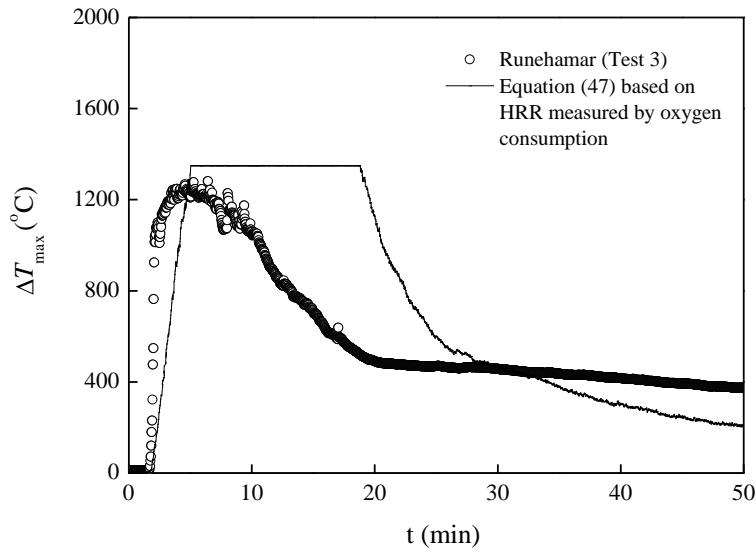


Figure 23 Comparison of calculated transient maximum temperature beneath the ceiling with data from Runehammar Test 3.

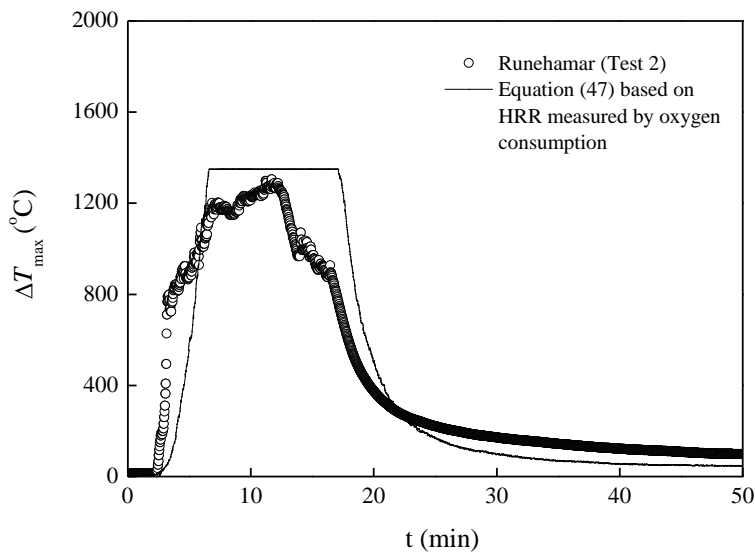


Figure 24 Comparison of calculated transient maximum temperature beneath the ceiling with data from Runehammar Test 4.

3.1.6 Example of how to use the temperature correlation

The correlations defined by Equations (46) and (47) can be used to calculate the excess gas temperature as a function of the heat release rate. They can also be used to find the corresponding heat release rates, if one assume a standardized time-temperature curve and a given tunnel geometry and ventilation conditions. To demonstrate this, the following fictive example is given.

- An HGV vehicle (Heavy Goods Vehicle trailer) is assumed to start to burn. The ignition can be related to the fact that one vehicle starts to burn (a tire fire or engine problems). The fire can also be regarded as a fire that starts due to a collision of two HGVs. We assume that the tunnel is designed for the RWS curve and want to see what heat release rate this would correspond to and also if the fire duration is assumed to be 120 minutes, what is the corresponding fire load.
- The tunnel height at its maximum is 6 m and the width is 12 m at its widest part. The height from the bottom of the fire load and up to the ceiling is 4.8 m.
- The radius of the fuel in the vehicle, b_{fo} , is 4 m.
- The longitudinal ventilation is assumed to be 3 m/s.
- The fire is assumed to be fuel controlled.
- The ambient conditions are 10 °C.

Firstly we assume $V' > 0.19$ since $Q(t)$ is unknown. This means that Equation (47) is used here. The corresponding heat release rate is found in Figure 25. Then we calculate V' using Q_{max} , which turns out to be greater than 0.19. This means at any time in this scenario, $V' > 0.19$ is fulfilled, which verifies the first assumption. For data with a temperature over 1150 °C, it is difficult to determine in which region it lies. However, it is clear that the calculated heat release rate is the minimum value required to obtain such a high temperature.

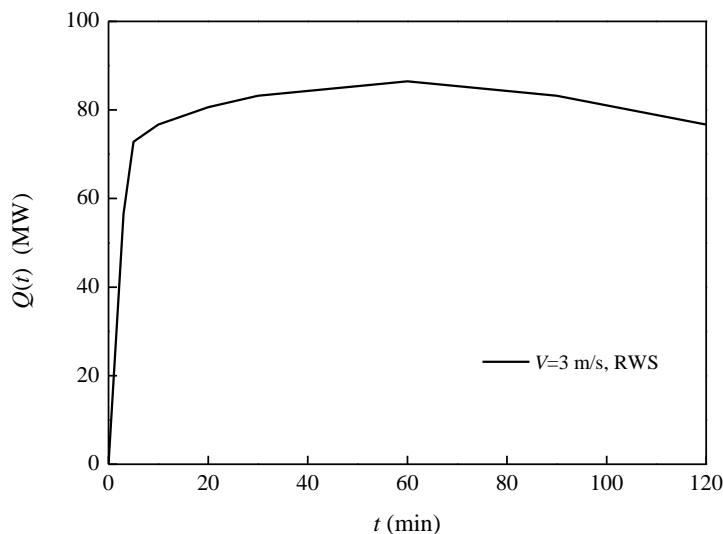


Figure 25 The calculated heat release rate corresponding to a RWS curve in a tunnel that is 6 m high and with ventilation of 3 m/s.

If we integrate the curve we find the total energy to be 581 GJ. This would correspond to at least two HGVs. A reasonable conclusion is that this tunnel would be designed to a fire that can resist a collision between two HGVs, and the fire can be very intense for up to 120 minutes. This shows the practical implication of using Equations (46) and (47). These equations become a key to relate information between the standardized time-temperature curves and the fire load in terms of the heat release rate and total energy found in the fire load.

3.2 Position of maximum temperature beneath tunnel ceiling

As discussed previously, the position of the maximum temperature beneath the tunnel ceiling is directly related to the flame angle defined in a tunnel fire. In this report, these two parameters have been analyzed together based on experimental data from SWJTU tests in model Tunnel A and model Tunnel B. The reason why data from these tests are used for the analysis of the position of the maximum temperature is due to the high number of thermocouples installed at the ceiling. The intervals between two thermocouples for analysis of the position of the maximum temperature in Tunnel A and Tunnel B are 50 mm and 100 mm respectively.

3.2.1 Position of maximum temperature

According to the theoretical analysis in Chapter 2, the flame angle approaches a constant value if the ventilation velocity is relatively low compared to the heat release rate, and it varies as power law of the dimensionless ventilation velocity if the ventilation velocity increases. The flame angle seems insensitive to the heat release rate for a large fire. The flame angle can be expressed as follows:

$$\sin \varphi = \frac{H_{ef}}{L_{traj}} = \begin{cases} 1, & V' \leq 0.19 \\ (5.26V')^{-3/5}, & V' > 0.19 \text{ \& } Q^* \leq 0.15 \\ 0.25(b_{fo}V'^3 / H)^{-1/5} & V' > 0.19 \text{ \& } Q^* > 0.15 \end{cases} \quad (40)$$

Firstly, the effect of heat release rate is confirmed. Figure 26 shows the flame angles varying with the heat release rates. Figure 27 shows the flame angles independent of heat release rate for large fires. All the data used in these two figures come from a series of tests in Tunnel A. Comparing these two figures shows that, if the flame angles are assumed to be independent of heat release rate for large fires, the experimental data shows a much better trend, and also correlates with Equation (40) better.

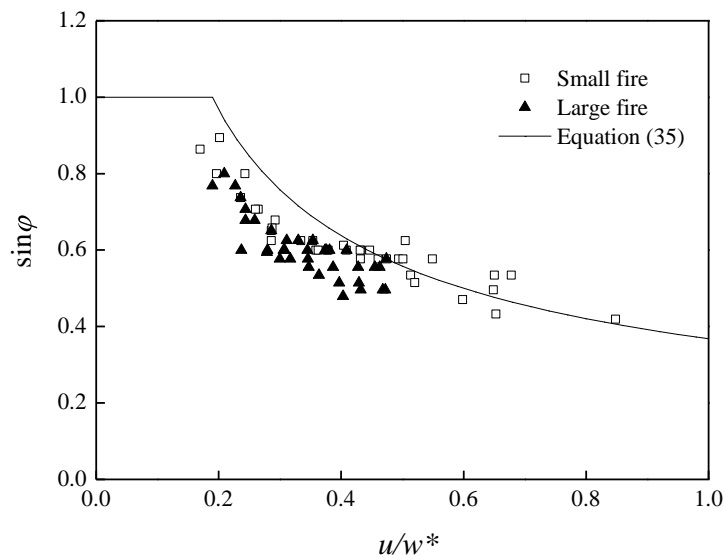


Figure 26 The flame angle and the dimensionless ventilation velocity with variant heat release rate for a large fire (Tunnel A).

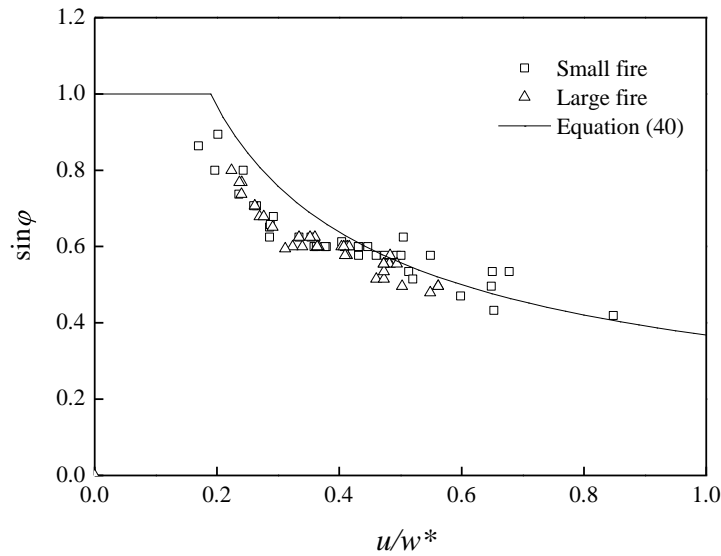


Figure 27 The flame angle and the dimensionless ventilation velocity independent of heat release rate for a large fire (Tunnel A).

This verifies the previous hypothesis that the flame angle, which is directly related to the position of maximum temperature, is independent of the heat release rate for a large fire in a tunnel.

Figure 28 shows how the flame angle varies with the dimensionless ventilation velocity, independent of the heat release rate for a large fire in Tunnel A and Tunnel B. All the data show a good trend and fits the proposed Equation (40) well.

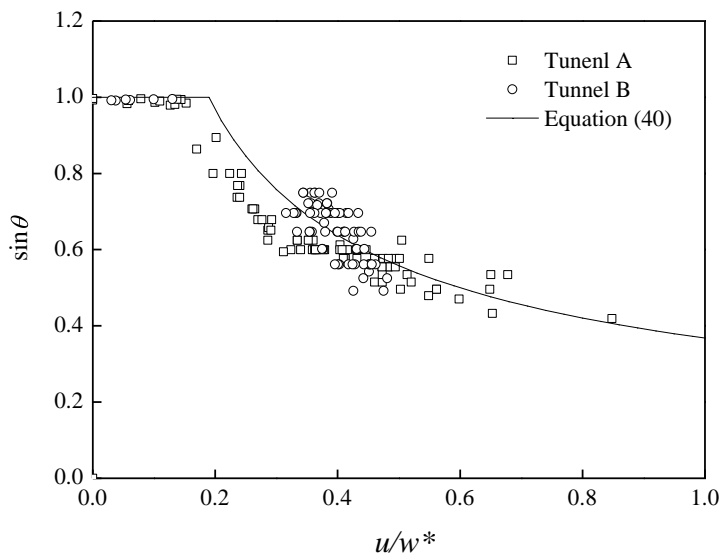


Figure 28 The flame angle and the dimensionless ventilation velocity independent of the heat release rate for a large fire (Tunnel A and Tunnel B).

A comparison between the measured positions of maximum temperature beneath the ceiling and calculated value based on Equation (40) is shown in Figure 29. All data points

are close to the equal line, which means Equation (40) can predict the position of the maximum temperature beneath the ceiling well.

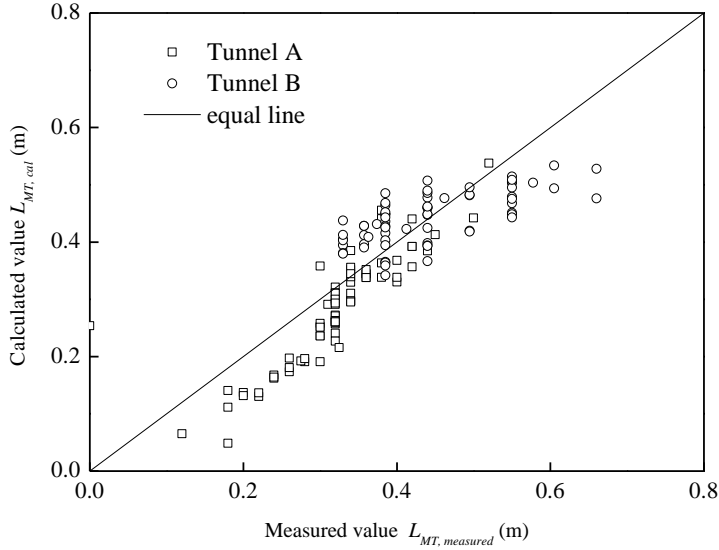


Figure 29 Comparison of measured position of maximum temperature with calculated value based on Equation (38).

3.2.2 Critical flame angle

According to the former theoretical analysis, the flame angle can be simply expressed as:

$$\sin \varphi_c = 0.42 \left(\frac{b_{fo}}{H} \right)^{-1/5} \quad (43)$$

This means that for a given tunnel and fire source, the flame angle is always the same, no matter whether the scenario is a large fire in a tunnel or not. The same condition is obtained for the position of the maximum temperature beneath the tunnel ceiling.

Figure 30 shows the comparison between the experimental data for the critical angle and the calculated values based on Equation (43). All the experimental data from SWJTU tests in Tunnel A and Tunnel B are plotted here. The ratios, b_{fo} / H , are almost of the same value, 0.20, both in Tunnel A and Tunnel B. This means the theoretical value of the flame angle in both tunnels is 33° . Comparing the experimental data of the critical angle with the calculated values based on Equation (43) shows there is a very good agreement between them. This strongly verifies the results of the theoretical analysis. The dotted line in Figure 30 can be simply expressed as:

$$\varphi_c = 33^\circ \quad (48)$$

It should, however, be pointed out that the effect of the geometry of the fire source on the flame angle is not considered in the tests. In order to understand this fully there is a need to do further research on this subject.

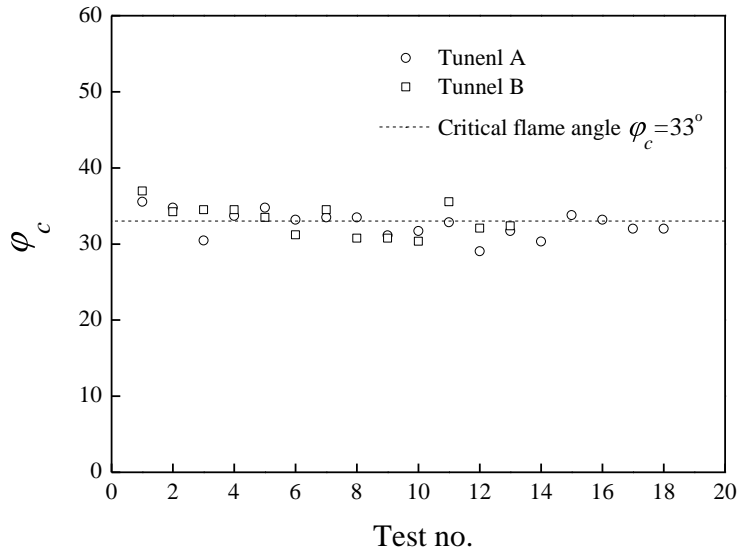


Figure 30 The critical flame angle in a ventilated tunnel fire.

3.2.3 Comparison with Raj et al's formulae

Figure 31 shows the comparison with Raj et al's formulae for the flame angle. It is shown that Raj et al's formulae overestimate the flame angle to some extent, and the proposed Equation (38) correlate better with the experimental data. Note that the flame angle in Raj et al's formulae is slightly different to the flame angle in a tunnel fire as discussed here. In a ventilated tunnel fire, the flame angle is defined based on the position of the maximum temperature beneath the ceiling. Therefore it is reasonable that the flame angle in a ventilated tunnel fire is slightly lower than the realistic flame angle.

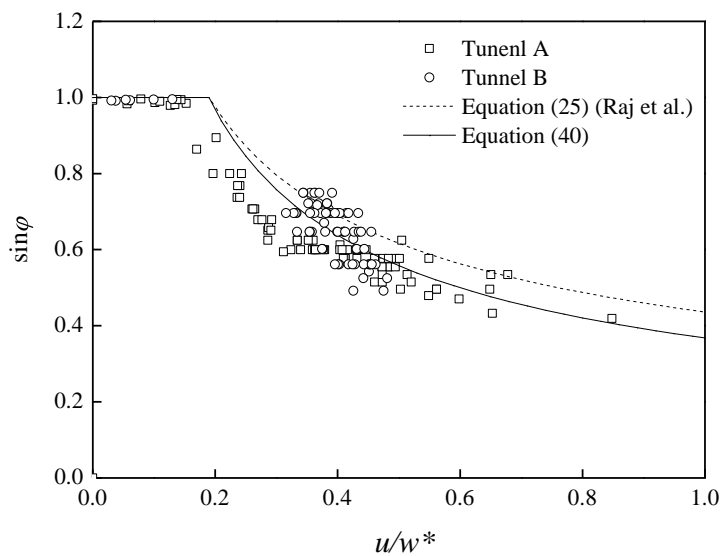


Figure 31 Comparison with Raj et al's formulae for flame angle.

3.2.4 Comparison with Kurioka's formulae

Comparison between the measured position of the maximum temperature beneath the ceiling and calculated value based on Kurioka et al.'s formulae is shown in Figure 32. As shown in Table 1, Kurioka et al. divided the maximum temperature into three regions, i.e. Region 1, 2 and 3, according to the value of the maximum temperature.

The data points in Figure 32 show some scattering trend. It is clear that the calculated position of the maximum temperature is much higher than the measured values in Kurioka et al.'s Region 1 ($\Delta T_{\max} \leq 250$), both for Tunnel A and Tunnel B. In their Region 3 ($\Delta T_{\max} \geq 550$), the calculated value is much lower than the corresponding measured value. Note that the data in Region III were obtained under low ventilation. This may mean that Kurioka's formula may underestimate the position of maximum temperature if the ventilation velocity across the fire is very low. The calculated values in their Region 2, i.e. ($250 < \Delta T_{\max} < 550$) correlate with the measured values much better than in other regions. It is also clearly shown that data points for different regions lie in different groups, and there appears to be no good continuity of equations between the different regions.

Comparing Figure 32 with Figure 29 shows that Equation (40) fit the test results concerning the position of maximum temperatures beneath the tunnel ceiling much better than Kurioka *et al.*'s formulae.

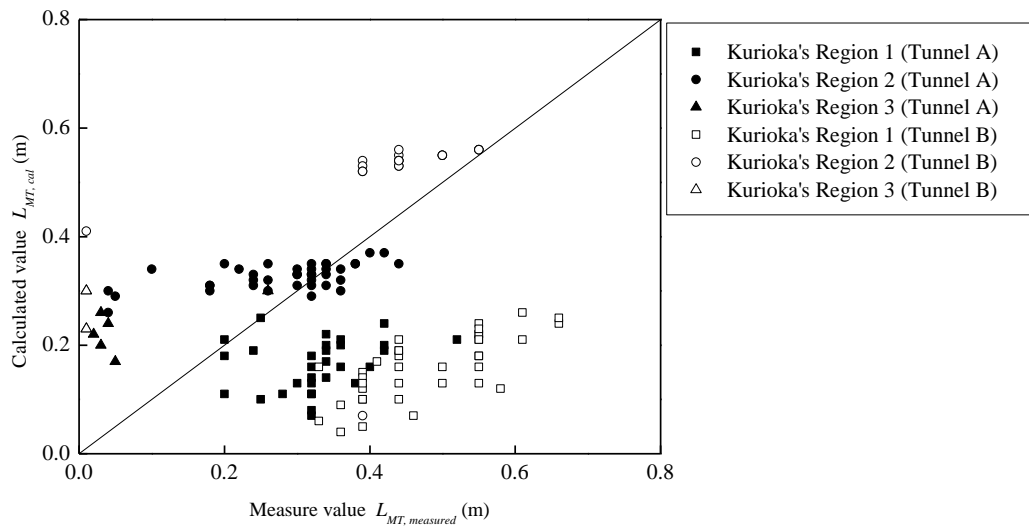


Figure 32 Comparison of measured positions of maximum temperature and calculated value based on Kurioka et al.'s formula.

4 Conclusions

A theoretical analysis of the maximum excess gas temperature beneath a tunnel ceiling and its position in the case of a tunnel fire has been presented. Large amounts of data from model scale tests and large scale tests were used to verify and improve the proposed model from the theoretical analysis.

Results of both the theoretical analysis and experimental data show that the maximum temperature can be divided into two regions according to the dimensionless ventilation velocity, V' . The main parameters taken into account in the theoretical analysis include the heat release rate, the ventilation velocity, the effective tunnel height and the geometry of the fire source.

For a small fire in a tunnel, the maximum excess gas temperature beneath the tunnel ceiling increases linearly with the heat release rate and decreases linearly with the longitudinal ventilation velocity when the dimensionless ventilation velocity exceeds 0.19. When the dimensionless ventilation velocity is lower than 0.19, the maximum gas excess temperature beneath the tunnel ceiling varies as the two-thirds power of the heat release rate, independent of the longitudinal ventilation velocity. In both regions, the maximum gas excess temperature varies as a $-5/3$ power law of the effective tunnel height, i.e. the distance between bottom of the fire source and the tunnel ceiling.

For a large fire in a tunnel, i.e. when the flame impinges on the ceiling and crawls along the tunnel ceiling, it was found that the maximum excess gas temperature beneath the ceiling approaches a constant value, regardless of the ventilation velocity. However, the thermal properties of the tunnel structure, the presence of dripping and flowing water from cracks in the blasted rock tunnels, the duration of the high temperature (for example high heat release rate and low ventilation velocity) and the fuel type are all parameters that can influence the ultimate value of the maximum temperature. This means that the maximum excess gas temperature in the constant region is not a universal constant, but dependent on the specific conditions for any given tunnel fire. Based on the theoretical analysis and analysis of the experimental data, a correlation for the maximum excess gas temperature beneath the tunnel ceiling is proposed. The correlation is valid up to a given maximum excess gas temperature of 1350 °C. This value was found to be the upper limit for a maximum excess gas temperature obtained from large scale tunnel tests. It is, however, clear that the levels of maximum gas temperatures depends mainly on the heat release rate, the tunnel height alternatively the height between the ceiling and the burning object if the fire source is elevated from the road surface and the ventilation type and flow rate. Other factors that are less dominating but probably importance when concerning the level of maximum ceiling temperatures are the type of tunnel linings or tunnel construction (rock, concrete, cracked and leaky blasted rock) and the fuel type.

The fuel type can include vehicles, solid fuels or liquid fuels. Open solid fuels with no coverage or open liquid fires, were found to yield the highest maximum ceiling gas temperatures if the heat release rates are high enough. In the case of vehicles, the different types of exterior body types such as steel, aluminum or fibre glass which may affect the amount of convective and radiant heat towards the ceiling are important. This may affect the final value of the maximum ceiling gas temperature for the same level of heat release rates. Finally it was found the model scale tests results do not obtain higher temperatures than 1100 °C, i.e. they predict a lower maximum gas temperature than the large scale tests.

Based on Quintiere et al.'s excellent work, the formulae for predicting the position of maximum temperature beneath the ceiling was obtained. A flame angle has been defined here according to the position of the maximum temperature beneath the tunnel ceiling in a fire. The format of the obtained formulae is similar to Raj et al.'s formulae for flame angle, although these two flame angles are different due to the definition and the scenario. Both theoretical analysis and experimental data show that the flame angle defined here is directly related to the dimensionless ventilation velocity. Moreover, the flame angle seems insensitive to the heat release rate for a large fire in a tunnel, as does the back-layering length [23]. The reason is that these two terms are both related to the dimensionless ventilation velocity. A particularly interesting finding is that there seems to be a critical flame angle, which is defined as the flame angle at the critical condition that the back-layering just disappears. In other words, for a given tunnel and fire source, the flame angles at the critical condition are almost of the same value, independent of the heat release rate.

A comparison of the proposed formulae for the maximum excess gas temperature beneath the tunnel ceiling with transient data from model scale tests and large scale tests shows good agreement. This means that the maximum excess gas temperature beneath the ceiling in a tunnel fire can be estimated well if the heat release rate curve and the specific geometries of tunnel and fire source are known. The good correlation, between the proposed formulae for the maximum excess gas temperature beneath the ceiling and its position in a tunnel fire and the data from model scale tests and large scale tests, provides confirmation of the theoretical analysis.

5 References

1. Carvel R. O., Marlair G. *A history of fire incidents in tunnels*. In: Beard A. N. and Carvel R. O., Editors, *The Handbook of Tunnel Fire Safety*. London, Thomas Telford Publishing, 2008; 3-41.
2. ISO834-1. *Fire-resistance tests -Elements of building construction - Part 1: General requirements*. International Organization for Standardization. 1999.
3. EN1363-2. *Fire resistance tests - Part 2: Alternative and additional procedures*, European Committee for Standardization. 1999.
4. *Beproeving van het gedrag bij verhitting van twee isolatiematerialen ter bescherming van tunnels bij brand*, Instituut TNO voor Bouwmaterialen en Bouwconstructies, B-79-391, Delft, The Netherlands, 1979.
5. *Richtlinien für Ausstattung und Betrieb von Tunneln (RABT)*. Ausgabe 1985 ed., Forschungsgesellschaft für Straßen - und Verkehrswesen, 1985.
6. *Abschlussbericht zum BMVBS/BASt Forschungsvorhaben 15.263 R95E: Baulicher Brandschutz für Tunnel in offener Bauweise*. iBMBTU Braunschweig, März 1998.
7. *Abschlussbericht zum BMVBS / BASt Forschungsvorhaben 15.0391/2003/ERB: Brandschutzverhalten von selbstverdichtendem Beton (SVB) im Straßentunnelbau*. MFPA Leipzig, Dec. 2005.
8. Kurioka H., Oka Y., Satoh H., Sugawa O. *Fire properties in near field of square fire source withlongitudinal ventilation in tunnels*. *Fire Safety Journal*. 2003, 38: 319-340.
9. Hu L. H., Huo R., Peng W., Chow W. K., Yang R. X. *On the maximum smoke temperature under the ceiling in tunnel fires*. *Tunnelling and Underground Space Technology*, 2006; 21:650-655.
10. Li Y. Z., Lei B. and Ingason H. *The Maximum Temperature of Buoyancy-driven Smoke flow below the ceiling in Tunnel Fires*. *Fire Safety Journal*, 2009 (Submitted).
11. Hoult, D. P., Fay, J. A., and Forney, L. J. *A Theory of Plume Rise Compared with Field Observations*. *Journal of the Air Pollution Control Association*. 1969(19): 585-590.
12. Hoult D. P., and Weil J. C. *Turbulent plume in a laminar cross flow*. *Atmospheric Environment*. 1972, 6(8): 513-530.
13. Karlsson B., and Quintiere J. G. *Enclosure Fire Dynamics*. Washington: CRC Press, 2000.
14. Heskestad, G. "Fire Plumes," *SFPE Handbook of Fire Protection Engineering*. National Fire Protection Association, Quincy, MA, 1995.
15. Zukoski, E. E. *Smoke movement and mixing in two-layer fire models*. The 8th UJNR Joint Panel Meeting on Fire Research and Safety. Tsukuba. 1985.
16. Quintiere J. G., Rinkinen W. J., and Jones W. W. *The effect of room openings on fire plume entrainment*. *Combustion Science and Technology*. 1981; 26:193-201.
17. Raj P. P. K., Moussa A. N., and Aravamudau K. *Experiments involving pool and vapor fires from spills of liquidified natural gas on water*. Prepared for U.S. Dept. of Transportation, U.S. Coast Guard, Rept. No. CG-D-55-79.

18. Lönnermark, A. and H. Ingason. *The Effect of Cross-sectional Area and Air Velocity on the Conditions in a Tunnel during a Fire*. SP Report 2007:05. Borås, Sweden, SP Technical Research Institute of Sweden.
19. McCaffrey B. J. *Purely buoyant diffusion flames: some experimental results*. NBSIR79-1919. National Bureau of Standards. 1979.
20. Lönnermark A., Ingason H. *Gas temperatures in heavy goods vehicle fires in tunnels*. *Fire Safety Journal*. 2005(40): 506-527.
21. *Memorial Tunnel Fire Ventilation Test Program - Test Report*. Massachusetts Highway Department and Federal Highway Administration, 1995.
22. Ingason, H. and Li, Y. Z. *Model scale tunnel fire tests with point extraction ventilation*. SP Report 2010:03. SP Technical Research Institute of Sweden: Borås, Sweden.
23. Li Y. Z., Lei B. and Ingason H. *Study of critical velocity and backlayering length in longitudinally ventilated tunnel fires*. *Fire Safety Journal*. (Accepted)
24. Drysdale D. *An introduction to fire dynamics* (2nd Version), John Wiley & Sons, 1999.
25. Quintiere J. G. *Scaling application in fire research*. *Fire Safety Journal*. 1989; 15:3-29.
26. Heskestad G. *Modeling of enclosure fires*. 14th symposium on combustion. The Pennsylvania State University, USA, 1972. pp.1021-1030.
27. Heskestad G. *Physical modeling of fire*. *Journal of Fire and Flammability*. 1975; 6:253–273.
28. Ingason, H. *Model scale railcar fire tests*. *Fire Safety Journal*. 2007; 42:271-282.
29. Ingason, H. and Li, Y. Z. *Model scale tunnel fire tests with longitudinal ventilation*. *Fire Safety Journal*. (Accepted)
30. Ingason, H. *Model scale tunnel fire tests with longitudinal ventilation*. SP Report 2005:49. SP Swedish National Testing and Research Institute: Borås, Sweden.
31. Ingason, H., Werling, P. *Experimental study of smoke evacuation in a model tunnel*. FOA Defence Research Establishment. FOA-R--99-01267-311--SE, Tumba, Sweden, 1999.
32. Bettis, R. J., Jagger S. F. and Wu Y. *Interim validation of tunnel fire consequence models: summary of phase 2 Tests*. Health and Safety Executive Research and laboratory services division.1993.
33. Ingason H. *Fire testing in road and railway tunnels*. In: Apte V. B., Editor, *Flammability testing of materials used in construction, transport and mining*. Woodhead Publishing in materials and CRC Press. 2006, p231-274.
34. Haerter, A. *Fire tests in the Ofenegg tunnel in 1965*. International Conference on Fires in Tunnels, SP REPORT 1994:54, 195-214, Borås, Sweden, 10-11 October, 1994.
35. *Schlussbericht der Versuche im Ofenegg tunnel von 17.5 - 31.5 1965*. Kommission für Sicherheitsmassnahmen in Strassentunneln, 1965.
36. Pucher, K. *Fire Tests in the Zwenberg tunnel (Austria)*. International Conference on Fires in Tunnels, 187-194, Borås, Sweden, 1994.

37. *State of the road tunnel equipment in Japan - ventilation, lighting, safety Equipment*. Public Works Research Institute, Technical note, Vol. 61, Japan, 1993.
38. *Fires in transport Tunnels: report on full-scale tests*. edited by Studiengesellschaft Stahlanwendung e. V., EUREKA-Project EU499 : FIRETUN, Düsseldorf, Germany, 1995.
39. Ingason, H. *Heat release rate measurements in tunnel fires*. International Conference on Fires in Tunnels, 86-103, Borås, Sweden, 1994.
40. Steinert, C. *Smoke and Heat Production in Tunnel Fires*. The International Conference on Fires in Tunnels, 123-137, Borås, Sweden, 1994.
41. Lemaire, T., van de Leur, P. H. E., and Kenyon, Y. M. *Safety Proef: TNO Metingen Beneluxtunnel – Meetrapport*. TNO, TNO-Rapport 2002-CVB-R05572, 2002.
42. Lemaire, T., and Kenyon, Y. Large scale fire tests in the Second Benelux tunnel. *Fire Technology*. 2006(42): 329-350.
43. van de Leur, P. H. E., and Kenyon, Y. M. *Safety Proef: TNO Metingen Beneluxtunnel – Meetrapport*. TNO, TNO-Rapport 2002-CVB-R05572, 2002.
44. Ingason, H. and Lönnemark A., *Heat Release Rates from Heavy Goods Vehicle Trailers in Tunnels*. *Fire Safety Journal*, 2005(40):646-668.
45. Lönnemark, A., and Ingason, H. *Large Scale Fire Tests in the Runehamar Tunnel - Gas Temperature and Radiation*. International Symposium on Catastrophic Tunnel Fires (CTF), SP Report 2004:05. Borås, Sweden, 2004.

Appendix A Model scale tests

Many model scale tunnel fire tests have been conducted using scaling theories. Normally the influence of the thermal inertia of the involved material, the turbulence intensity and radiation are ignored, but the heat release rate, flow rates, the time and the fuel mass are conserved. The most commonly used scaling theory is the Froude scaling. Information about this scaling theory can be obtained from for example references [24-27]. Most of data from these model scale tests show that some tunnel fire characteristics, especially in the near field of the fire source, can be modelled well even in a tunnel with a scaling ratio of about 1:20. Data from model scale tunnel fire tests, as well as large scale data, are used in this report. In this chapter, a summary of all the model scale data on maximum gas temperature is given.

A1. SP model scale tests with longitudinal ventilation

Ingason [28-29] carried out 12 tests with wood cribs in a model tunnel (1:23) using longitudinal ventilation. The fire load was simulated with aid of wood cribs and the fire spread between two or three wood cribs with a free distance of 0.65 m (about 15 m in large scale) was tested. The tunnel itself was 10 m long, 0.4 m wide and 0.2 m high, as shown in Figure A1. The model was constructed using non-combustible, 15 mm thick, boards (Promatect H). The floor, ceiling and one of the vertical walls were built in Promatect H boards while the front side of the tunnel was covered with a fire resistance window glaze. The 5 mm thick window glaze (0.6 m wide and 0.35 m high) was mounted in steel frames which measured 0.67 m by 0.42 m.



Figure A1 A photo of a model-scale tunnel used by Ingason [28-29] for tests with longitudinal ventilation.

Longitudinal ventilation was established with aid of an electrical axial fan attached to the entrance of the model tunnel. Longitudinal wind velocities of 0 m/s and 0.62 m/s were

used in the test series. The fire load consisted of a wood crib (pine). In the longitudinal ventilation study two different types of wood cribs were used, wood crib A and wood crib B, respectively. The total weight of wood crib B ranged from 0,91 kg to 1,24 kg. The total fuel surface area of wood crib B was estimated to be 0.56 m². Two methods, i.e. mass loss method and oxygen consumption calorimetry, were used to determine the heat release rate in a tunnel fire.

Various measurements were conducted during each test, see Figure A2. The first wood crib was placed on a weighing platform (W), consisting of a scale attached by four steel rods to a free floating dried Promatect H board measuring 0,65 m long, 0,35 m wide and 0,12 m thick. The temperatures were measured with welded 0,25 mm type K thermocouples (TC). A bi-directional probe (BD) was placed at the centreline of the tunnel 8,72 m from the inlet (at pile B). Another bi-directional probe was placed upstream the fire at the centre of the cross-section and 1,15 m from the inlet. At three locations and flush to the floor board, water cooled heat flux meters of type Schmidt-Boelter were placed to record the total heat flux. The gas concentrations (O₂, CO₂ and CO) were measured 8,72 m from the entrance (at pile B) by two measuring probes consisting of open copper tubes (Ø 6 mm). They were located at two different heights, 0.10 m and 0.175 m above the floor. A bi-directional probe and a oxygen probe were mounted in the centre of the 0,25 m diameter steel exhaust duct on the floor. The weighing platform, the thermocouples, the pressure transducers, the gas analysers and flux meters were connected to IMP 5000 KE Solotron loggers. The data were recorded on a laptop computer at a rate of about one scan per second.

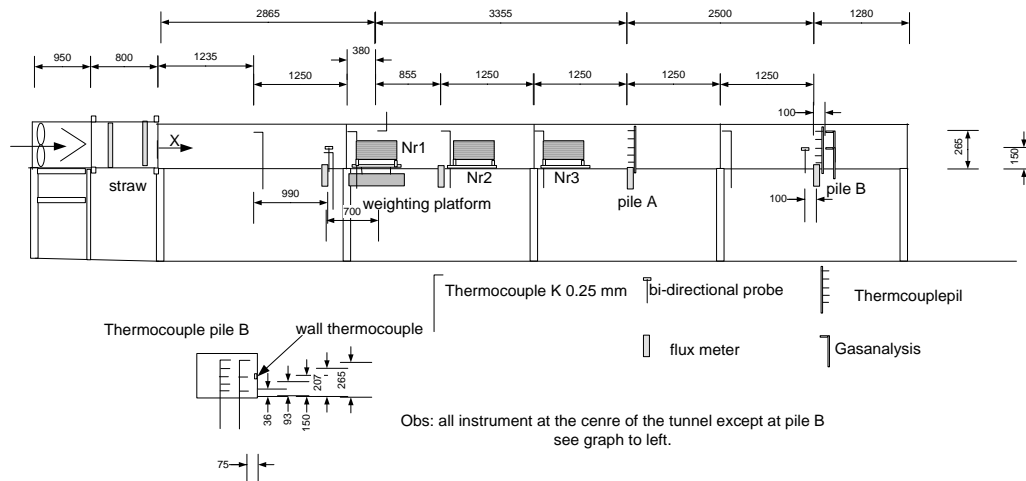


Figure A2 A schematic of the model-scale test-rig with longitudinal ventilation.

Relevant data from SP longitudinal ventilation tests are listed in Table A1. The heat release rate was normally predicted by fuel mass loss which was measured by weighing platform, except for tests with several wood cribs burning together in which the heat release rate was measured by oxygen calorimetry technique.

Table A1 Relevant data from the SP longitudinal ventilation tests [28-29].

Test nr	Geometry of cross-section width×height	Fuel type	u	T_0	Q_{max}	T_{max}	H_f	b_{fo}
	m		m/s	°C	kW	°C	m	m
1	0.4×0.3	wood crib	0.54	20	135.3	1014.3	0.25	0.166
2	0.4×0.3	wood crib	0.87	20	151.8	871.0	0.25	0.166
3	0.4×0.3	wood crib	0.45	20	254.7	1033.4	0.25	0.166
4	0.4×0.3	wood crib	0.46	20	320.8	1057.7	0.25	0.166
5	0.4×0.3	wood crib	0.56	20	145.8	942.8	0.25	0.166
6	0.4×0.3	wood crib	0.45	20	117.9	1007.9	0.25	0.166
7	0.4×0.3	wood crib	0.38	20	141.3	994.9	0.25	0.166
8	0.4×0.3	wood crib	0.54	20	142.8	1046.8	0.25	0.166
9	0.4×0.3	wood crib	0.76	20	288.4	1179.5	0.25	0.166
10	0.4×0.2	wood crib	0.54	20	103.7	979.7	0.15	0.144
11	0.4×0.2	wood crib	0.86	20	106.7	1060.9	0.15	0.144
12	0.4×0.2	wood crib	0.33	20	102.2	1030.8	0.15	0.144

A2. SP model scale tests with extraction ventilation

Ingason and Li [23] presented 12 tests with point extraction ventilation system in a scale of 1:23. The fire load was simulated with aid of wood cribs. The parameters tested were the longitudinal ventilation rate, the arrangement of the exhaust openings and the exhaust capacity. Moreover, the fire spread between wood cribs with a free distance of 0.65 m (about 15 m in large scale) was tested.

The point extraction ventilation system was tested under different fire and flow conditions using either forced longitudinal ventilation or natural ventilation. The study focuses on single and two point extraction systems. The maximum heat release rate, fire growth rate, maximum excess temperature beneath the ceiling, flame length and heat flux were analyzed using relationships obtained from theoretical considerations.

This series of tests was carried out in a similar tunnel as model scale tests with longitudinal ventilation, except the exhaust vents arranged at the ceiling of the 0.2 m high model tunnel, see Figure A3.

The extraction ventilation channel, with a height of 0,1 m and the same width as the tunnel, was above the ceiling, as shown in Figure A3. The total flow rate through the extraction vents used were 0.06 m³/s, 0.10 m³/s and 0.15 m³/s.. The number of exhaust openings that were used in the tests varied between 1 and 2. In other words, in these tests the single point extraction system and two point extraction system were aimed at. The area of the openings were 0,026 m² and 0,052 m², respectively.

The centre of the ceiling openings (vents) were placed with an equal distance of 2,17 m. The distance from the tunnel entrance ($x=0$) to the centre of the opening Nr 1 was 1,7 m.

The size of the openings varied during the tests; $0,026 \text{ m}^2$ and $0,052 \text{ m}^2$, respectively. The width of the openings was kept the same during all tests, $0,026 \text{ m}$, whereas the length (in the x-direction) was varied between $0,1 \text{ m}$ and $0,2 \text{ m}$, respectively. The steel duct was connected to the central ventilation system used to ventilate the fire test hall. The flow rate was predetermined before each test by regulating a valve between the steel duct and the central ventilation system. The total exhaust airflow in the steel duct was $0,06 \text{ m}^3/\text{s}$, $0,10 \text{ m}^3/\text{s}$, and $0,15 \text{ m}^3/\text{s}$. Wood crib B were used to simulate the fire source, which was designed to correspond to a HGV (Heavy Goods Vehicle) fire load in large scale.

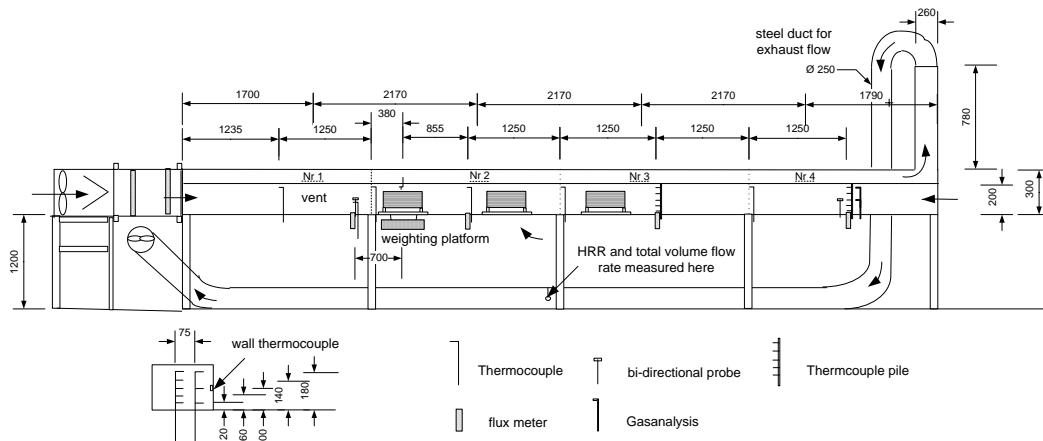


Figure A3 A schematic of the model-scale test-rig with extraction system.

Relevant data from SP extraction ventilation tests are listed in Table A2. The heat release rate was normally predicted by fuel mass loss which was measured by weighing platform, except for tests with several wood cribs burning together in which the heat release rate was measured by oxygen calorimetry technique.

Table A2 Relevant data from the SP longitudinal ventilation tests [30].

Test nr	Geometry of cross-section width×height	Fuel type	u	T_0	Q_{max}	T_{max}	H_f	b_{fo}
	m		m/s	°C	kW	°C	m	m
1	0.4×0.2	wood crib	0.61	20	97.7	1056.9	0.15	0.144
2	0.4×0.2	wood crib	0.25	20	65.1	860.2	0.15	0.144
3	0.4×0.2	wood crib	0.26	20	52.6	768.3	0.15	0.144
4	0.4×0.2	wood crib	0.32	20	86.6	1009.3	0.15	0.144
5	0.4×0.2	wood crib	0.34	20	57.6	939.3	0.15	0.144
6	0.4×0.2	wood crib	0.59	20	83.9	1037	0.15	0.144
7	0.4×0.2	wood crib	0.57	20	158.3	1004.5	0.15	0.144
8	0.4×0.2	wood crib	0.58	20	190.6	981.7	0.15	0.144
9	0.4×0.2	wood crib	0.4	20	51.4	1033.1	0.15	0.144
10	0.4×0.2	wood crib	0.52	20	52.6	813.5	0.15	0.144
11	0.4×0.2	wood crib	0.36	20	57.6	808.8	0.15	0.144
12	0.4×0.2	wood crib	0.38	20	75.2	909	0.15	0.144

A3. FOA/SP model scale tests

FOA/SP model scale tests [31] were performed in a 1 m high, 2 m wide, 12 m long model tunnel in 1999, as shown in Figure A4 and Figure A5. The main objective of this experimental study is to investigate the influence of longitudinal ventilation on the efficiency of thermal and mechanical ventilation in tunnels using exhaust shafts and to obtain well defined experimental data for validation of CFD models. Totally 36 tests were performed, i.e. 26 with thermal ventilation and 10 with mechanical ventilation.

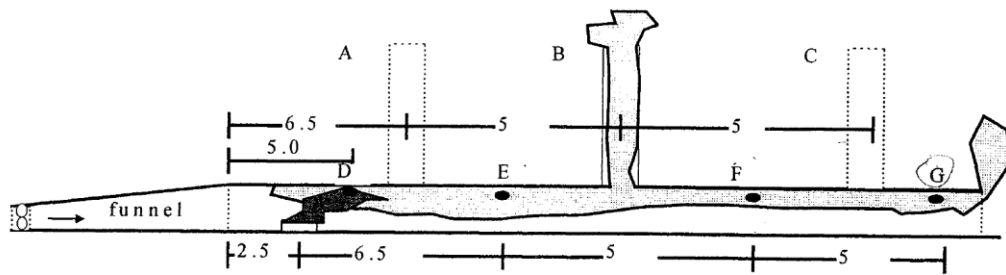


Figure A4 The FOA/SP experimental set up. All dimensions are in meter.



Figure A5 The model tunnel in the FOA/SP tests.

The material of the walls, floor and ceiling consisted of a 12 mm Promatec fibre-silica board – except for one side-wall which consisted of 5 mm thick fire resistant window glass. The window was used to visually document from one end of the tunnel. Two different pan sized were used, 0.33×0.33 m and 0.4×0.4 m, respectively. The exhaust ventilation arrangement and the longitudinal velocity was varied. Different number of thermal shafts were mounted along the tunnel at locations A, B and C. For tests with mechanical ventilation, only the shaft B was connected to a exhaust fan, and shaft A and C were closed.

A specially designed funnel shaped tunnel was attached to one end of the tunnel in order to create a uniform flow over the cross-section at the tunnel entrance. The other end of the tunnel was fully open. Before the ignition of the fire source, there is a forced flow inside the tunnel.

Ceiling temperature was measured at the centre line and 0.1 m beneath the ceiling by K-type thermocouples with a wire diameter of 0.25 mm. Measurements were also performed at four different locations downstream of the fire source, locations D, E, F and G, at heights of 0.1, 0.3, 0.5, 0.7, 0.9 m above the tunnel floor. The velocity was measured 0.1 m below the ceiling at station D, E, F, and G and 0.5 m above floor at station E and F.

Kerosine was used as fuel. The heat release rate was estimated by measurement of fuel mass loss. Circulate water was used to cool the rim and obtain a steady mass burning rate during the pool fire tests.

Relevant data from FOA/SP tests are listed in Table A3. Two types of ventilation system-natural ventilation and mechanical ventilation were tested in this series of tests. In a natural ventilation system, the tunnel portals on both sides were opened to model the real scenario of tunnel fire and the ventilation velocity across the fire is considered as zero here.

Table A3 Relevant data from FOA/SP tests [31].

Test nr	Ventilaiton	Fuel type	u	T_0	Q_{max}	T_{max}	H_f	b_{fo}
			m/s	°C	kW	°C	M	m
1	natural	kerosine	0	20	38.3	283.2	0.95	0.186
3	natural	kerosine	0	20	32.7	262.7	0.95	0.186
7	natural	kerosine	0	20	53.4	343.1	0.95	0.226
14	natural	kerosine	0	20	71.9	310.7	0.95	0.226
17	natural	kerosine	0	20	79.4	291.3	0.95	0.226
21	natural	kerosine	0	20	33.9	261.1	0.95	0.186
27	natural	kerosine	0	20	61.62	209	0.95	0.226
28	natural	kerosine	0	20	45.03	150	0.95	0.226
2	mechanical	kerosine	1	20	42.3	103.5	0.95	0.186
4	mechanical	kerosine	0.5	20	30.9	113.7	0.95	0.186
5	mechanical	kerosine	0.75	20	29.9	106.5	0.95	0.186
6	mechanical	kerosine	1	20	40.9	106.7	0.95	0.186
8	mechanical	kerosine	1	20	54.9	150.5	0.95	0.226
9	mechanical	kerosine	0.75	20	50.3	185.3	0.95	0.226
10	mechanical	kerosine	0.5	20	46.6	158.7	0.95	0.226
11	mechanical	kerosine	0.5	20	48.7	179.3	0.95	0.226
12	mechanical	kerosine	0.75	20	49	155.2	0.95	0.226
13	mechanical	kerosine	1	20	59	155.4	0.95	0.226
15	mechanical	kerosine	0.5	20	48.3	176.7	0.95	0.226
16	mechanical	kerosine	1	20	70	150.2	0.95	0.226
18	mechanical	kerosine	1	20	57.4	155.9	0.95	0.226
19	mechanical	kerosine	0.75	20	49.2	162.3	0.95	0.226
20	mechanical	kerosine	0.5	20	51.8	202.5	0.95	0.226
22	mechanical	kerosine	1	20	41	99.6	0.95	0.186
23	mechanical	kerosine	0.75	20	29.9	100.9	0.95	0.186
24	mechanical	kerosine	0.5	20	30.3	122.9	0.95	0.186
25	mechanical	kerosine	0.5	20	51.3	197	0.95	0.226
26	mechanical	kerosine	1	20	55.9	153.7	0.95	0.226
29	mechanical	kerosine	1	20	59.64	159	0.95	0.226

30	mechanical	kerosine	1	20	56.49	160	0.95	0.226
31	mechanical	kerosine	1	20	56.09	154	0.95	0.226
32	mechanical	kerosine	1	20	64.39	157	0.95	0.226
33	mechanical	kerosine	0.5	20	53.33	200	0.95	0.226
34	mechanical	kerosine	1	20	59.25	161	0.95	0.226
35	mechanical	kerosine	2	20	74.26	96	0.95	0.226
36	mechanical	kerosine	2	20	73.87	112	0.95	0.226

A4. SWJTU model scale tests

Li et al [10][23] conducted a series of fire tests in two model tunnels, i.e. Tunnel A and Tunnel B. Each small-scale test rig consisted of a 12 m long model tunnel, a 5.25 m long air supply duct, and a static pressure box, as shown in Figure A6 and Figure A7. The cross sections of these tunnels can be seen in Figure A8. The study aims at the control of smoke flow, the interaction of the fire plume with the ventilated flow, and the temperature distribution.

The static pressure box, which was used to smooth the turbulence of the air flow, was a cuboid with 1 m length, 0.5 m width and 0.5 m height. The fire source in Tunnel A was a 100 mm diameter porous bed burner, and that in Tunnel B was a 150 mm diameter burner, with its top surface set at floor level. Propane was used as fuel, and its gas flow rate was metered by a rotameter with 1 % accuracy. The heat release rate was estimated by the gas flow rate. The ventilation flow rate in the tunnel was metered by a vortex flowmeter with a range of 30~540 m³/h and 1 % accuracy. The ventilation velocity was calculated by dividing the volumetric flow rate by the tunnel cross-sectional area.

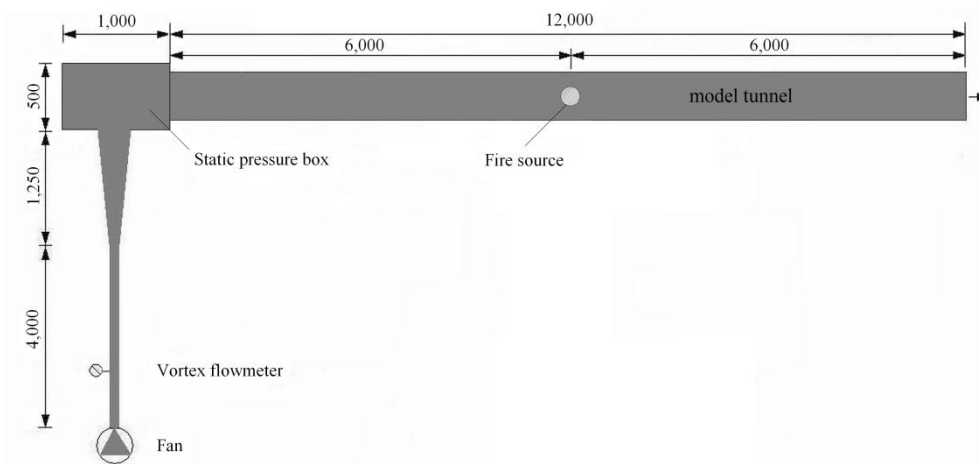
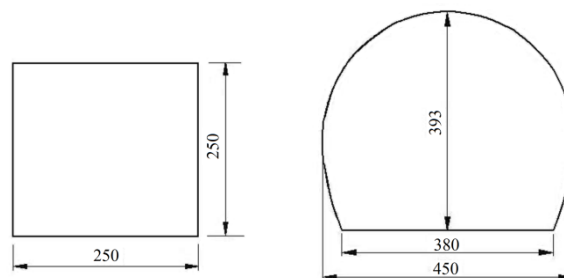


Figure A6 Schematic diagram of SWJTU model scale tests (Dimensions in mm)



Figure A7 A photo of the model-scale test bed (Dimensions in mm)



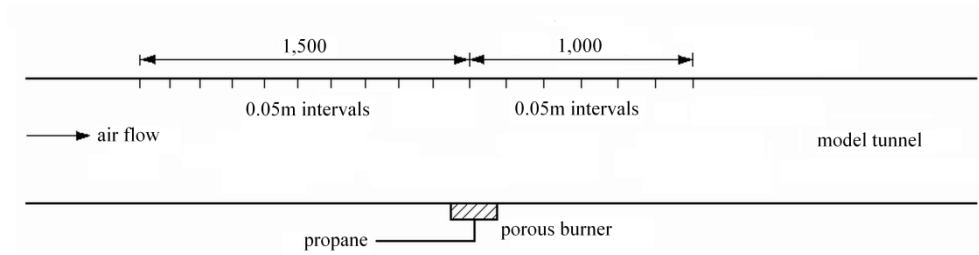
(a) Tunnel A

(b) Tunnel B

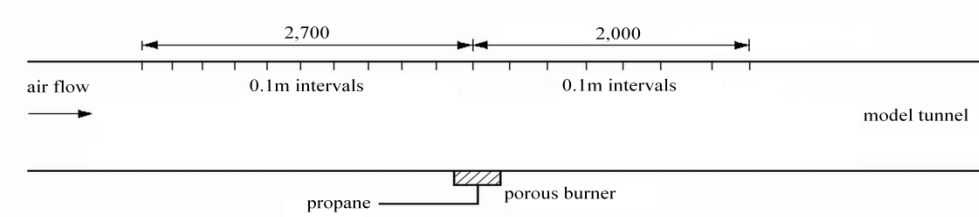
Figure A8 Cross-sections of model tunnels (Dimensions in mm)

Gas temperature below the ceiling was measured by using K-type stainless steel-sheathed thermocouples with a diameter of 1.0 mm. The layout of thermocouples is shown in Figure A9. The thermocouples were mounted centre line 10 mm below the centre line of the ceiling in Tunnel A, and 20 mm below the ceiling in Tunnel B.

After series of tests carried out in Tunnel A and Tunnel B, a model vehicle 8 m long, 0.15 m wide and 0.2 m high was positioned symmetrically inside Tunnel B. The model consisted of 1 mm thick steel. The aim was to analyse the effect of obstruction in the tunnel on the critical velocity and back-layering length. The model vehicle represented an obstruction, such as a passenger train or road vehicles in a queue situation. The distance from the bottom of the model vehicle to the tunnel floor was 40 mm. The model vehicle occupied about 20 % of the tunnel cross-section area. For practical reasons, and because we did not want the heat release rate to be affected, as it would be if placed inside the model, the fire source was retained at the same location beneath the model, allowing the flames to surround the model.



(a) Tunnel A



(b) Tunnel B

Figure A9 Positions of thermocouples (Dimensions in mm)

Due to too many experimental data from SWJTU tests are used in this report, only part of them are listed in Table A4. The ambient temperatures were approximately 20 °C and 10 °C in the series of tests in Tunnel A and Tunnel B, respectively.

Table A4 Relevant data from SWJTU tests [10][23].

Test nr	Test tunnel	u	Q _{max}	T _{max}	H _f	b _{fo}
		m/s	kW	°C	M	m
1	Tunnel A	0.70	4.35	216.5	0.25	0.05
2	Tunnel A	0.59	4.35	256.0	0.25	0.05
3	Tunnel A	0.52	4.35	271.7	0.25	0.05
4	Tunnel A	0.46	4.35	266.3	0.25	0.05
5	Tunnel A	0.40	4.35	276.3	0.25	0.05
6	Tunnel A	0.36	4.35	296.0	0.25	0.05
7	Tunnel A	0.69	5.16	271.2	0.25	0.05
8	Tunnel A	0.59	5.16	313.1	0.25	0.05
9	Tunnel A	0.51	5.16	313.8	0.25	0.05
10	Tunnel A	0.42	5.16	330.7	0.25	0.05
11	Tunnel A	0.34	5.16	358.7	0.25	0.05
12	Tunnel A	0.72	6.05	297.2	0.25	0.05
13	Tunnel A	0.66	6.05	321.8	0.25	0.05
14	Tunnel A	0.58	6.05	360.8	0.25	0.05
15	Tunnel A	0.48	6.05	363.5	0.25	0.05
16	Tunnel B	0.33	1.97	53.9	0.393	0.075
17	Tunnel B	0.36	1.97	49.1	0.393	0.075
18	Tunnel B	0.38	1.97	45.8	0.393	0.075
19	Tunnel B	0.40	1.97	45.5	0.393	0.075
20	Tunnel B	0.42	1.97	38.6	0.393	0.075
21	Tunnel B	0.41	3.48	89.4	0.393	0.075

22	Tunnel B	0.43	3.48	77.7	0.393	0.075
23	Tunnel B	0.45	3.48	72.8	0.393	0.075
24	Tunnel B	0.47	3.48	68.1	0.393	0.075
25	Tunnel B	0.50	3.48	59.0	0.393	0.075
26	Tunnel B	0.43	4.58	106.8	0.393	0.075
27	Tunnel B	0.45	4.58	95.0	0.393	0.075
28	Tunnel B	0.49	4.58	97.3	0.393	0.075
29	Tunnel B	0.53	4.58	88.5	0.393	0.075
30	Tunnel B	0.55	4.58	79.4	0.393	0.075

A5. HSE model scale tests

After the Channel Tunnel fire, HSE conducted a series of experiments by which the validity of the CFD methodology could be assessed [32].

The cross-section of the model tunnel is of the similar geometry as the Channel Tunnel with a scaled-down ratio of 1:3, shaped to BS227 Colliery Arch with an area of 5.6 m². The tunnel height is 2.44 m, and the maximum width is 2.75 m. The surface of tunnel is made of reinforced concrete with thickness of 0.41 m over the first 184 m, 0.48 m between 184 m and 275 m, and 0.57 m from 275 m to the open end at 366 m. The southern end of the model tunnel was open through the test series, and the northern end wall held an inlet for the main ventilation fan.

The tunnel walls in the immediate vicinity of the fire site and at a given distance downstream of the fire, were provided with fire protection, in order to protect the structural integrity of the model tunnel. The fireproofing was achieved using mineral fibre sheeting, marketed as Conlit 100, which was 25 mm thick and coated on one side with a thin aluminium foil.

In order to simulate the complexity of flows around a fire in the forward section of an HGV shuttle train, models of some of the vehicles were constructed at a suitable scale to fit the gallery. The scaled-down ratio of HGV shuttle model is 1:2.8.

Liquid pools and wood cribs were used as fuels. The heat release rate ranges from 0.9 MW to 18.9MW.

A wide range of instruments were deployed to measure the various parameters that are of interest in this fire situation, i.e. measurement of temperature, velocity, smoke density, heat flux and gas.

Relevant available data from the series of HSE tests are listed in Table A5.

Table A5 Relevant data from the SP longitudinal ventilation tests [32].

Test nr	u m/s	T_0 °C	Q_{max} MW	T_{max} °C	H_f M	b_{fo} m
1	0.5	10	4.1	1140	2.04	1.5
2	1.1	10	3.5	914	2.04	1.5
3	1	10	11.5	900	2.04	1.5
4	1.1	10	11.5	942	2.04	1.5
5	1.1	10	11.4	974	2.04	1.5
6	1.1	10	5.3	1171	2.04	1.5
8	1	10	4.9	1142	2.04	1.5

Appendix B Large scale tests

In order to examine the validity of the theoretical correlations developed in chapter 2, it is necessary to summaries all the large scale tests carried out and can be of relevance for determining the maximum gas temperature. In the following a summary of numerous large scale data is presented as well as necessary information on geometry, fuel sources, ventilation conditions and instrumentation. In Table B1, a list of the large scale tests used in the analysis are given [33].

Table B1 Scientifically aimed large-scale fire tests since the middle of 1960s.

Test program, country, year	No of tests	Fire source	Tunnel cross-section (m ²)	Tunnel height (m)	Tunnel length (m)	Measure-ments	Range of peak HRR (MW)
Ofenegg, Switzerland, 1965	11	Gasoline (6.6, 47.5, 95 m ²)	23	6	190	T,CO,O ₂ ,v, visibility	11-80
Glasgow, 1970	5	Kerosine (1.44 , 2.88, 5.76 m ²)	39.5	5.2	620	T, OD	2 - 8
Zwenberg, Austria, 1974 - 1975	30	Gasoline (6.8, 13.6 m ²), wood and rubber	20	3.9	390	T,CO,CO ₂ , NO _x ,CH, O ₂ , v, OD	8 – 21
P.W.R.I, Japan, 1980	16	Gasoline (4, 6 m ²), passenger car, bus	57.3	~6.8	700	T, CO, CO ₂ , v, OD, radiation	Pool : 9 – 14*
P.W.R.I, Japan, 1980	8	Gasoline (4 m ²), bus	58	~6.8	3277	T, CO, CO ₂ , O ₂ , v, OD, radiation	Pool: 9 Bus unknown
EUREKA 499, Norway, 1990 - 1992	21	Wood cribs, heptane, cars, metro car, rail cars, HGV trailer and mockup	25 – 35	4.8 ~5.5	2300	HRR,T,CO, m,CO ₂ ,O ₂ ,S O ₂ ,C _x H _y , NO,visibilit y,soot,m,v	2 – 120
Memorial, USA, 1993-1995	98	Fuel oil (4.5 – 45 m ²)	36 and 60	4.4/ 7.9	853	HRR, T,CO, CO ₂ ,v, isibility	10 - 100
2nd Benelux tunnel, The Netherlands, 2002	14	n-heptane +toulene, car, van, HGV mock up	50	5.1	872	HRR, T, m, radiation, v, OD, visibility	3 - 26
Runehamar tunnel, Norway 2003	4	Cellulose, plastic, furniture	32 - 47	4.7 ~5.1	1600	HRR,T,PT, CO,CO ₂ ,O ₂ ,HC N,H ₂ O, isocyanates, OD, radiation	70 – 203

HRR=Heat Release Rate, m=mass loss rate, T=temperature, PT=Plate Thermometer, CO=Carbon monoxide, CO₂=Carbon dioxide, CH= Hydrocarbon, HCN=cyanide, H₂O=water vapour, v=velocity, OD=Optical density, visibility=cameras for smoke registration,

In the following a more detailed description of the most important large scale tests, together with data presented in the summary by Ingason [33], is given.

B1. Ofenegg tunnel 1965

The first large scale tunnel fire test series to obtain scientific and engineering information was carried out in the Ofenegg tunnel in Switzerland, in 1965 [34][35]. These tests were carried out in order to study the ventilation capacities (natural, longitudinal, semi-transverse) in the case of a fire, especially in case of a gasoline tank fire. The tests were expected to give information on the hazardous level for tunnel users, possibilities to rescue people and the impact on tunnel construction and installations. The tunnel used was a single track railway tunnel (23 m², 3.8 m wide and 6 m high), with wall located 190 m from the one portal and the ceiling was 6 m high with a rounded top. By closing the cross-section the test tunnel became a dead end tunnel of 190 m in length.

A total of 11 tests were performed using gasoline pool fires on a concrete trough with the edge placed 131.5 m from the open entrance. The other end (190 m) was bricked up. The sizes of the pools used were 6.6 m², 47.5 m² and 95 m², respectively, with the smallest representing the contents of the fuel tanks of two cars and the largest a substantial spill from a gasoline tanker. The width of the trough (fuel pan) was 3.8 m and the length of the trough varied; 1.7 m, 12.5 m and 25 m, respectively.

In tests with natural ventilation, all ventilation ducts were closed and also the rear access door. In a longitudinal ventilation test, the air was blown in through the rear end duct system. In a semi-transverse ventilation test, a sheet metal air duct was set up with side-openings every 5 m along most of the test tunnel including the fire site. The fresh air supply rate was equal to 0.25 m³/s. Ventilation velocity can be calculated for a longitudinal ventilation system, or estimated to be 0 for a natural ventilation system. However, for a semi-transverse ventilation system, it is hard to determine it.

Ingason estimated the HRR and tabulated maximum gas temperatures and velocity from each test. The results are presented in Table B2, together with estimation of the effective tunnel height, H_{ef} , and diameter of the fuel, b_{fo} . The estimation is based on the measured fuel flow rates for each test and a assumed combustion efficiency of 0.8 in the tunnel and a heat of combustion of 43.7 MJ/kg. The maximum ceiling temperature obtained was 1325 °C and the average HRR was estimated to be 70 MW. With a natural ventilation or semi-transverse ventilation the temperatures were slightly lower or about 1200 °C and the average HRR was between 33 MW to 39 MW. In general we see that the maximum ceiling temperature varies between 450 °C ~ 1325 °C for average HRRs between 12 MW and 70 MW. Clearly, the temperatures are not only dependent on the level of the HRR but also by the ventilation conditions.

Table B2 Relevant data from the Ofenegg tunnel tests in 1965 [34-35].

Test nr	Type of ventilation	Fuel type	Air supply ventilation	u	T_0	Q_{max}^*	T_{max}	$H_{f^{**}}$	$b_{fo^{**}}$
			m ³ /s	m/s	°C	MW	°C	m	m
1	Natural	Gasoline	0	0	16	16	710	5.5	1.43
2	Semi-trans.	Gasoline	15	-	17.5	12	830	5.5	1.43
2a	Longitud.	Gasoline	39	1.70	11	14	450	5.5	1.43
5	Natural	Gasoline	0	0	10	39	1200	5.5	3.89
6	Semi-trans.	Gasoline	15	-	10	33	1180	5.5	3.89
7a	Longitud.	Gasoline	39	1.70	11.3	70	1325	5.5	3.89
9	Natural	Gasoline	0	0	4.6	35	1020	5.5	5.50
10	Semi-trans.	Gasoline	6	-	9	32	850	5.5	5.50

* HRR is calculated by $HRR = \eta \dot{m}_f'' A_f \Delta H_c$ where η is the combustion efficiency, \dot{m}_f'' is the burning rate per square meter, A_f is the fuel area and ΔH_c is the heat of combustion. We assume

$\eta = 0.8$ in tests with natural and semi-transverse ventilation and $\eta = 0.9$ in the tests with longitudinal

ventilation. The heat of combustion ΔH_c is assumed to be equal to 43.7 MJ/kg and the fuel density is assumed to be 740 kg/m³ [33].

** based on estimation by the authors

B2. Zwenberg 1975

A decade after the Ofenegg tunnel tests, a new test series was carried out in the Zwenberg tunnel in Austria 1975 [36]. The aim was to investigate the effects of different types of ventilation (longitudinal, semi-transverse and transverse ventilation) on the distribution of smoke (visibility), heat and toxic gases and the effects of heat on the ceiling construction and the exhaust fans.

The tests were carried out in an abandoned railway tunnel owned by the Austrian Railways. The tunnel was 390 m long with a cross-section of 20 m² (traffic space) and a ventilation duct of 4 m². The tunnel gradient was 2.5% from the south to the north portal. The tunnel height up to the ventilation duct was 3.8 m and the tunnel width was 4.4 m. Fully transverse ventilation system was installed in the test tunnel, designed for a supply of 30 m³/s of fresh air and for the same quantity of exhaust air. An injection fan installed near the southern portal was designed to provide a longitudinal flow up to 7 m/s in the traffic space. Every 6 m alternately a fresh air opening and a polluted air opening were installed.

The fire source was located 108 m from the south portal. It consisted of 12 individual concrete trays in two rows with a total volume of 900 litres liquid (gasoline, diesel) corresponding to a surface area of 20 m² where the internal measures of each tray was 1 m wide and 1.7 m long. Only four trays (beside each other) were used in the standards

test (6.8 m²) and six in the large tests (13.6 m²). A total of 46 measuring points for temperature were mounted, 11 for air and gas velocities, 19 for gas sampling (O₂, CO₂, CO, CH and NO_x) and 7 for visibility observations. Total of 30 tests, see Table B3, were performed using gasoline pools of 3.4 m², 6.8 m² and 13.6 m², respectively. The majority of the tests, 23 ‘standard fire’ tests, were run using 4 trays with a fuel area of 6.8 m² and 200 litre of fuel. This fire size was found to be sufficient to obtain useful data and avoid damages on the installation. In the tests with the ‘standard fire’ following parameters were varied:

The selected combination of different test parameters can be obtained from the second column in Table B3 (identification code of test 210) according to the following system:

X1 – X2 – X3 – X4 – X5

where

X1 – Location of fresh air supply:

U=from below

O=from above

X=no supply

X2 – Quantity of exhausted air:

1= nominal quantity 30 m³/s

1/3= 10 m³/s

X3 – Supplied quantity of fresh air:

1=nominal quantity 30 m³/s

1/3= one third of 30 = 10 m³/s

X4 – Longitudinal ventilation velocity in the traffic space (m/s)

X5 – Conditions in the traffic space:

F=free cross-section

A=test models in the traffic space

Transverse ventilation system has both extraction and supply of air. Fully transverse ventilation have equal amount of exhaust and supply air. The HRR estimation and maximum gas temperature in Table B3 are obtained from Ingason [33].

Table B3 Relevant data from the Zwenberg tunnel fire tests in 1975.

Test no.	Identification code of test	Test condition	Fuel type	U	T_0	Q_{max}^{**}	T_{max}	$H_{f^{***}}$	$b_{f_0^{***}}$
				m/s	°C	MW	°C	m	m
101	U-1-1-7-F	TOF	gasoline	7	NA	8	NA	3.63	1.04
102	U-1-1-2.5-F	TOF	gasoline	2.5	NA	12	NA	3.63	1.47
103	U-1-1-0-F	FTV		0	12	10	904	3.63	1.47
104	U-1-1/3-0-F			0	10	12	1240	3.63	1.47
105	X-1-0-0-F	EO		0	12	13	1320	3.63	1.47
106	0-1-1/3-0-F			0	8	12	1222	3.63	1.47
107	0-1-1-0-F	FTV		0	10	8	1080	3.63	1.47
203	U-1-1-0-A	FTV		0	8	10	856	3.63	1.47

204	U-1-1/3-0-A			0	10	10	1118	3.63	1.47
205	X-1-0-0-A	EO		0	10	12	1254	3.63	1.47
206	0-1-1/3-0-A			0	8	12	1318	3.63	1.47
207	0-1-1-0-A	FTV		0	10	8	1134	3.63	1.47
208	U-0-1-0-A	STV		0	12	8	822	3.63	1.47
209	U-1-1-2-A	FTV		2	14	13	663	3.63	1.47
210	U-1-1/3-2-A			2	12	12	563	3.63	1.47
211	U-1-1-2-F	FTV		2	12	12	670	3.63	1.47
212	X-0-0-2-A	PLV		2	14	12	623	3.63	1.47
213	X-0-0-4-A	PLV		4	12	12	312	3.63	1.47
214	X-0-0-0-A	EO		0	16	9	1000	3.63	1.47
215	0-1-1-2-F	FTV		2	12	12	612	3.63	1.47
216	0-0-1-0-A	STV		0	13	9	893	3.63	1.47
217	0-0-1/3-0-A	STV		0	11	8	1165	3.63	1.47
218	0-1-1/3-2-A			2	10	11	623	3.63	1.47
219	X-1-0-2-A	EEO		2	6	11	675	3.63	1.47
221	X-1-0-2-A	EO		0	8	7	723	3.63	1.47
220	X-1-0-0-A	EO	Diesel	0	8	10	643	3.63	1.47
301	X-1-0-0-A	EO	gasoline	0	6	20	1332	3.63	2.08
302	0-1-1/3-0-A			0	6	17	1320	3.63	2.08
303	0-0-1/3-0-A			0	8	21	1330	3.63	2.08

* TF – Test of Facility (preliminary tests)

EO – Extraction Only

PLV – Pure Longitudinal Ventilation

FTV – Fully Transverse Ventilation

STV – Semi Transverse Ventilation

EEV – Enlarged Extraction Opening

** Ingason assumed in tests with natural and semi-transverse ventilation and in the tests with longitudinal ventilation, the heat of combustion was equal to 43.7 MJ/kg and the fuel density was 740 kg/m³ [33].

NA=Not Available

*** based on estimation by the authors

B3. P.W.R.I 1980

The Public Works Research Institute (P.W.R.I.) in Japan performed two series of large-scale tests [37]. The first test series were carried out in P.W.R.I.'s own full-scale test tunnel facility and the second test series was carried out on the Chugoku Highway in the Kakeitou Tunnel. The full-scale tunnel at P.W.R.I. site has a total length of 700 m, a cross sectional area of 57.3 m² (H=6.8 m) and is equipped with ventilation and sprinkler facilities. The Kakeitou tunnel has a total length of 3277 m, a cross-sectional area of 58 m² (H=6.7 m), and is equipped with ventilating and sprinkler facilities. The majority of the experiments were conducted in the full-scale tunnel at P.W.R.I. but also in the Kakeitou tunnel. The main purpose of using the long tunnel was to determine the environment for people evacuating from tunnels.

The fire source consisted of gasoline pool (gasoline) fires, passenger cars and large-sized buses. Gasoline pool fires of 4 m² and 6 m² were used to generate a HRR equal to the fire for large-sized vehicle, large-sized buses and passenger cars. The pool fires were applied in order to accomplish steady and repeatable fires, which may not be the case in tests

using real motor vehicles. Several real motor vehicles were, although used for confirmation of the results. Four to six sets of gasoline fire pools (trays) were arranged for fires, each having four 0.25 m² (a total of 1 m² fuel surface area) fire trays in one set. Further, 18 litres of gasoline was uniformly placed in each fire tray in order to maintain almost the same burning rate for about 10 minutes after ignition. In the tests with passenger cars, doors of the driver's seat were left half-opened, while other doors and windows were closed. Approximately 10 to 20 litres of gasoline were put in the fuel tank of the passenger cars. For large-sized buses, the entrance door, exit doors and the window next to the driver's seat were fully opened, and 50 litres of light oil was put in the fuel tank. With respect to passenger cars and buses, pieces of cloth soaked in advance in a small amount of gasoline were placed on the rear seats and ignited. A comprehensive instrumentation was used in these test series. The gas temperatures (84 points in the Kakei tunnel), concentrations of smoke (78 points in the Kakei tunnel), gas velocities (5 points), concentrations of O₂, CO gases (1 and 3 points, respectively), radiation (1 point) and burning velocity (mass loss rate) were measured.

No HRR measurements were carried out in these tests. The fuel mass loss rate of the pool fires was measured as a reduction in the level of fuel. It is reported that at 1 m/s longitudinal velocity the mass fuel rate was 0.63 cm/min (77.7 g/m² s assuming 740 kg/m³ for gasoline) and 1.24 cm/min (152.9 g/m² s) at 4 m/s. The authors refer to outside door test yielding 0.42 cm/min (51.8 g/m² s). These burning rates can be compared to values given in Table B2 (Ofenegg) and Table B3 (Zwenberg). At low velocities the values are in the same order, whereas at high wind velocity it is about factor of two higher. On passenger cars the burning rate was reported to be 7.4 kg/min (0.15 kg/s) at 1 m/s and 10 kg/min (0.17 kg/s) at 4 m/s. Assuming an average heat of combustion of 30 MJ/kg this would correspond to 4.4 MW and 5 MW, respectively. The burning rate of the seats in the buses was reported to be 6.9 to 8.1 kg/min (0.11 and 0.14 kg/s).

The ventilation system was able to create a longitudinal flow up to 5 m/s. The influence of the temperature due to the fire was found to be only limited to the nearby areas of the fire. In Table B4 a summary of all peak HRRs and ceiling temperatures is given. The data show clearly the effects of the longitudinal flow on the peak temperature in the ceiling. Higher velocity tends to lower the ceiling temperature due to dispersion of the hot air. It was not possible to extract any information about the flame lengths from the information available. An estimation of the free flame height for the pool fires used in this test series indicates that the flames were not impinging on the ceiling. The ceiling temperatures given in Table B4 confirm these calculations.

Table B4 The test programme for the P.W.R.I. test series in Japan 1980 [37].

Test nr.	Test tunnel	Fuel type	u	Q_{max}^*	T_{max} (+ 5 m)	H_f^{***}	b_{fo}^{**}
			m/s	MW	°C	m	m
1	P.W.R.I., 700m	gasoline	0.65	9.6	252	6.55	1.13
2	“	gasoline	5	9.6	41	6.55	1.13

5	“	gasoline	2	14.4	429	6.55	1.38
17	Takei,3277m	gasoline	0	9.6	511	6.55	1.13
18	“	gasoline	2	9.6	199	6.55	1.13
19	“	gasoline	5	9.6	69	6.55	1.13

* Based on estimation and not measurements. Due to the good ventilation condition we assume free burning conditions i.e. 2.4 MW/m² for gasoline (0.055 kg/m² s -43.7 MJ/kg [33])

** based on estimation by the authors

B4. EUREKA EU499 tests 1990 – 1992

The EUREKA EU499 test program was performed in an abandoned tunnel named Repparfjord Tunnel in northern Norway [38-40]. The tunnel was 2.3 km long with a gradient less than 1%, running north south from the main portal to a vertical shaft of 90 m height (cross-section of the shaft was 9 m²). The cross section of the tunnel was horseshoe shaped to rectangular with a flattened roof. The tunnel is approximately 5.3 to 7.0 m wide with a maximum height in the centre between 4.8 m and 5.5 m.

The test programme included 21 large-scale tests, which were carried out in 1990, 1991 and 1992. The majority of the tests were performed in year 1992 as can be observed in Table B5. The main objectives of the EUREKA EU499 test program were to investigate the fire behaviour of different type of fuels including real vehicles. Also to seek the possibilities of escape and rescue, and fire extinguish to see the damage of tunnel structure caused by fires. The fire behaviour of trains and HGVs revealed by these tests has had major effects on many design studies of large tunnel projects today.

The main results of the EUREKA EU499 project relates to the unique data of measured HRR for real vehicles where the oxygen consumption calorimetry was applied for the first time in large-scale tunnel tests. It also contained well-defined fire sources such as wood cribs and heptane pool fires, which are very valuable for scientific analysis of the results. The wood crib tests showed a tendency of increased fire growth rate with increased ventilation rate whereas it was not as apparent for the peak HRR. Results showed that generally the temperature of vehicles with body structure, which can melt away, e.g. the aluminium subway coach and the school bus (GFRP), could reach ceiling temperatures from 800 up to 1060 °C and HRR of 29 – 43 MW (tests 7, 11 and 14). For trains with steel body structure the HRR was less than 19 MW and the fire duration longer and the ceiling temperatures tended to be lower than 800 °C (tests 4, 5, 12 and 13). For the passenger car, the highest temperature was between 210 and 480 °C and the HRR was up to 6 MW (tests 3 and 20). The same tendency about the influence of the body type on the results is found for the plastic car and the steel body passenger car. The estimated flame lengths are given in Table B5 as towards the portal and towards the vertical shaft. It is based on 600 °C flame tip obtained from maximum temperature graphs as a function of the distance from the centre of the fire.

The EUREKA tests show the importance of the glazed windows on the fire growth in the steel body trains. The fire growth rate is apparently governed by the sequence and timing of the window cracking. This can be shown by analysing the temperature development inside the train compartments. The type of interior material (former or new design) appears not to be as eminent for the fire growth as expected. The type of body and the quality of the windows appears to be more important than the type of interior materials. For a heavy goods load (furnitures), which is not contained by any steel or aluminium body, the corresponding data were about 1000 °C and a HRR of 120 – 128 MW.

Table B5 Relevant data from the EUREKA EU499 test serie [38-40].

Test nr.	Fuel type	u	Q_{max}	T_{max} (0 m)	T_{max} (+10 m)	H_{f*}	b_{fo*}
		m/s	MW	°C	°C	M	m
7	School bus (GFRP)	0.3	29	810	690	4.6	3.27
8	Wood cribs no 3.	0.3	9.5	NA	480	4.8	0.90
9	Wood cribs no 4.	3.5	18	NA	440	4.8	0.90
10	Wood cribs no 5.	4.5	13	NA	290	4.8	0.90
11	1.5 rail cars F2Al+F7 (Aluminium+steel)	3.5	43	980	950	4.1	3.91
12	Rail car F2St (steel)	0.5	19	650	840	4.1	4.98
13	Rail car F1 (steel)	0.5	13	450	720	4.1	4.98
14	Metro car F4 (Aluminium)	0.5	35	810	1090	4.1	4.08
15	Mixed load simulating truck load	0.7	16.5	NA	400	4.5	2.93
16	1 m ² heptane pool no 1.	1.25	9	540	NA	4.8	0.56
17	1 m ² heptane pool no 2.	1.75	8	400	340	4.8	0.56
20	Private car (plastic)	0.5	6	480	250	4.5	1.60
21	Heavy Goods Vehicle (HGV) with furnitures	5	128	925	970	4.2	2.93

* based on estimation by the authors

B5. Memorial Tunnel tests 1993 – 1995

The Memorial Tunnel Fire Ventilation Test Program (MTFVTP) consisted of a series of large-scale fire tests carried out in an abandoned road tunnel [21]. Various tunnel ventilation systems and configurations of such systems were operated to evaluate their respective smoke and temperature management capabilities. The Memorial Tunnel test program was performed in a two-lane, 853 m long and 8.8 m wide road tunnel built in 1953, taken out of traffic 1987 and was a part of the West Virginia Turnpike. The tunnel has a 3.2 % upgrade from south to north portal. The tunnel was originally designed with a transverse ventilation system, consisting of a supply fan chamber at the south portal and an exhaust fan chamber at the north portal. An overhead air duct, formed by a concrete

ceiling 4.3 m above the roadway, was split into supply and exhaust section by a vertical concrete dividing wall. In some of the tests the horizontal ceiling was removed in order to put in place 24 reversible jet fans in-group of three equally spaced over the tunnel. The cross-section changed from rectangular shape with cross-sectional area of 36.2 m² to more of a horse shoe shape with an height of 7.8 m and a cross-sectional area of 60.4 m². These fans had a 56 kW motor and an outlet velocity of 34.2 m/s and a volume flow of 43 m³/s. They were designed to withstand air temperatures of about 300 °C.

The test programme consisted of 98 tests where the type of ventilation, fuel size and sprinklers were changed. The ventilation systems tested include longitudinal ventilation system, fully transverse ventilation system, semi-transverse ventilation system, etc. The results from some typical tests with different ventilation systems are listed in Table B6.

Table B6 The Memorial Tests program with different type of ventilation system.

Test nr.	Fuel type	Ventilation system	u	Q_{max}	T_{max}	$H_{f^{**}}$	$b_{fo^{**}}$
			m/s	MW	°C	M	m
101CR	diesel	FTV*	-	10	579.7	3.64	1.20
103	diesel	FTV*	-	20	1368.2	3.64	1.69
113A	diesel	FTV*	-	50	1369.9	3.64	2.66
217A	diesel	PTS/EV*	-	50	1347.2	3.64	2.66
238A	diesel	TZPTV*	-	50	1224.6	3.64	2.66
239	diesel	TZPTV*	-	100	1298.3	3.64	3.76
312A	diesel	PTV-SPE*	-	50	1302.2	3.64	2.66
313A	diesel	PTV-SPE*	-	50	811.0	3.64	2.66
401A	diesel	PTV-OEP*	-	50	1082.8	3.64	2.66
318A	diesel	PSPEO*	-	50	1236.3	3.64	2.66
501	diesel	Natural*	0.6	20	492.0	7.14	1.69
502	diesel	Natural	1.0	50	952.3	7.14	2.66
605	diesel	Longitudinal*	1.8	10	177.8	7.14	1.20
606A	diesel	Longitudinal	1.5	10	197.9	7.14	1.20
607	diesel	Longitudinal	1.75	20	366.3	7.14	1.69
610	diesel	Longitudinal	2.5	50	528.3	7.14	2.66
612B	diesel	Longitudinal	2.5	50	561.0	7.14	2.66
615B	diesel	Longitudinal	2.0	100	1086.1	7.14	3.76
618A	diesel	Longitudinal	2.25	20	367.2	7.14	1.69
621A	diesel	Longitudinal	2.5	100	816.6	7.14	3.76
623B	diesel	Longitudinal	1.8	20	384.3	7.14	1.69
624B	diesel	Longitudinal	1.8	50	720.3	7.14	2.66
625B	diesel	Longitudinal	2.0	100	1067.2	7.14	3.76

* FTV – Full Transverse Ventilation

PTS/EV – Partial Transverse Supply/Exhaust Ventilation

TZPTV – Two-Zone Partial Transverse Ventilation

PTV-SPE – Partial Transverse Ventilation with Single Point Extraction

PTV-OEP – Partial Transverse Ventilation with Oversized Exhaust Ports

PSPEO – Point Supply and Point Exhaust Operation.

Natural – Natural Ventilation

Longitudinal – Longitudinal Ventilation

**based on estimation by the authors

The tunnel was equipped with instrumentation and recording equipment for data acquisition. Sensors measuring air velocity, temperature, carbon monoxide (CO), carbon dioxide (CO₂) and total hydrocarbon content (THC) were installed at 12 cross-sections along the tunnel. In total there were approximately 1400 measuring points, each point was recorded once every second during the test (the test time ranged from about 20 to 45 minutes).

Ventilation system effectiveness in managing smoke and temperature movement was tested for the in advance calculated fire sizes (nominal): 10, 20, 50 and 100 MW. The corresponding fuel surface area is 4.5 m², 9 m², 22.2 m² and 44.4 m², respectively, meaning an average heat release rate of 2.25 MW/m². The fire source consisted of low-sulfur No 2 fuel oil in different pools (diesel). In addition to varying the fire size, systematic variations were made in airflow quantity, longitudinal air velocity near the fire, and fan response time for each ventilation system. Tests were also conducted to assess the impact of longitudinal air velocities on the effectiveness of a foam suppression system. Various smoke management strategies and combinations of strategies were employed, including extraction, transport, control direction of movement, and dilution to achieve the goals of offsetting buoyancy and external atmospheric condition and to prevent backlayering (critical velocity).

B6. 2nd Benelux tests 2002

Fourteen large-scale tests were carried out in the Second Benelux Tunnel in the Netherlands in 2002 [41-43]. The tests were designed to assess the tenability conditions for escaping motorists in case tunnel fire and to assess the efficiency of detection system, ventilation system and sprinkler system for numerous type of fire sources. These were pool fires, passenger cars, a van and mock-ups with truckloads. Temperatures, radiation levels and optical densities in the tunnel were measured, as well as smoke velocities and heat release rates.

The tests were carried out in a sink tunnel outside Rotterdam. In Table B7 results from these tests are given. The tunnel has a rectangular cross section with a height of 5.1 m and a width of 9.8 m and a length of about 900 m. Before the tests, the tunnel ceiling and part of the walls were sprayed with insulation in order to enhance the fire resistance of the tunnel structure in accordance with standard procedures for new tunnels in the Netherlands. In preparation for the tests, the walls, ceiling and floor of the tube were covered with additional fire protection cladding over lengths of 35 m upstream and 35 m downstream of the fire. The tunnel has a maximum slope of 4.4 % and was equipped with longitudinal ventilation. A total of six jet fans were installed at the upstream portal of the

tunnel in order to create air velocities up to 6 m/s. The test site was located at 265 m from the downstream portal.

The test program included 4 pool fire tests (Tests 1 ~ 4) with ventilation velocities between 0 m/s to 6 m/s. The pool fires consisted of a mixture of 60 % n-heptane and 40% toluene. The pool fire source consisted of two and four fuel pans, respectively, where each pan measured 1.8 m long and 1 m wide and the fuel level was 0.5 m above the road surface. The total fuel surface was 1.8 m² in tests 1 and 2 and 7.2 m² in tests 3 and 4.

The fire source used in tests 5 to 10 is cars and covered truckloads. Each truckload consisted of 800 kg wooden pallets (total of 36 EURO-pallets, 4 piles with 9 pallets in each pile), with four tyres placed on the top. The fire load was mounted in a on a mock-up of a truck with a cover of tarpaulin were the rear end was open. The total length of the mock-up was 4.5 m, the width was 2.4 m and the height was 2.5 m. The longitudinal ventilation was varied between 0 m/s to 6 m/s.

In tests 11 to 14, different sprinkler systems were activated after a few minutes in a range of 4 min to 14 min. Therefore only results from tests 1 to 10 are listed in Table B7. The velocities in tests with natural ventilation are measured upstream of the fire sources. In tests 1 to 4 with pool fires the vertical distance between the fire source centre and the ceiling is lower as shown in Table B7.

In all the tests, except for the fuel pans, the fire sources were mounted on a weighing platform in order to measure the HRR. The HRR for the pans was obtained from the mass loss rate of the supply fuel tank. The centreline temperatures were measured at five different heights at distance of 10 m, 20 m and 50 m upstream the fire and at 10 m, 20 m, 50 m and 200 m downstream the fire. The radiation heat flux from the fire was measured with cooled heat flux meters at eye-level at distance of 5 m, 10 m and 20 m from the fire centre. Ventilation velocities were measured at three positions upstream of the fire with hot wire anemometers and at three positions downstream the tunnel using bi-directional probes.

Table B7 The test program for the 2nd Benelux Tunnel tests [41-43].

Test nr.	Fire source	Type of ventilation	E_{tot}	u	T_0	Q_{max}	T_{max}	$H_{f^{**}}$	$b_{fo^{**}}$
			GJ	m/s	°C	MW	°C	m	m
1	n-heptane/ toluene 1.8 m ²	No LTV	NA*	1.5	13	4.1	218	4.6	0.76
2	n-heptane/ toluene 1.8 m ²	LTV	NA	2	15	3.5	220	4.6	0.76
3a	n-heptane/ toluene 7.2 m ²	No LTV	NA	1.7	12	11.5	470	4.6	1.51
3b	n-heptane/ toluene 7.2 m ²	LTV	NA	5	12	11.5	250	4.6	1.51
4	n-heptane/ toluene 7.2 m ²	LTV	NA	5	11	11.4	210	4.6	1.51

5	Passenger car	No LTV	NA	1	10	NA	230	4.3	1.85
6	Passenger car	No LTV	NA	1.5	10	4.9	210	4.3	1.85
7	Passenger car	LTV	NA	6	10	4.8	110	4.3	1.85
8	36 wood pallets, 4 tyres	No LTV	~10	1.5	10	13.2	400	4.3	1.85
9	36 wood pallets, 4 tyres	LTV	~10	5.3	10	19.5	290	4.3	1.85
10	36 wood pallets, 4 tyres	LTV	~10	5	10	16.2	300	4.3	1.85

*NA=Not available.

**based on estimation by the authors

B7. Runehamar 2003

Large-scale tunnel tests were carried out with HGV-trailer cargos in the Runehamar tunnel in Norway [44][45]. The tunnel is a two-way asphalted road tunnel that was taken out of use and is 1600 m long, 6 m high and 9 m wide, with a slope varying between 0.5 - 1 %. The tunnel was a blasted rock-tunnel with a cross-section varying between 47 – 50 m².

In total four tests were performed with fire in a HGV-trailer mock-up. In Table B8 results from these tests are given. The specific commodities used consisted of four different materials, each representing a category of material typically found in the cargo of a HGV-trailer. These commodities were: standardized wood pallets, plastic pallets made of polyethylene (PE), a standardized test commodity consisting of polystyrene cups (PS) in compartmented cardboard cartons and polyurethane mattresses (PUR). In total four tests were performed. In three tests mixtures of the various cellulosic and plastic materials were used, and in one test a commodity consisting of furniture and fixtures was used. A polyester tarpaulin covered the cargo in each test. The HGV trailer mock-up was 10.45 m long, 2.9 m wide and 4.5 m high with the trailer floor at 1.1 m above the road surface.

In Test 1 the fire load consisted of 11 tonnes of wooden and plastic pallets. At a distance of 15 m from the downstream side (rear end of the trailer-mockup) there was a target consisting of one pallet row of the same test commodity as used in test. In Test 2 the fire load consisted of 6.9 tonnes of wooden pallets and mattresses (include a target at 15 m). In Test 3 the fire load consisted of 8.5 tonnes of furniture on wooden pallets including the target at 15 m. In this test the fire load had 10 tyres (800 kg) positioned around the frame at the locations where they would be on a real HGV trailer. In Test 4 the fire load consisted of 2.8 tonnes of plastic cups in cardboard boxes on wooden pallets (no target used in this test). In each test the amount (mass ratio) of plastic materials was estimated to be about 18-19%.

In each test, two fans positioned near the tunnel portal were used to generate a longitudinal airflow, this was about 3 m/s (centreline) at the start of each test but reduced to about 2.4 -2.5 m/s once the fires became fully involved. At the location of the fire

experiments which was approximately 1 km into the tunnel, a 75 m length of the tunnel was lined with fire protective panels (Promatect T), this reduced the cross-sectional area of the tunnel to 32 m² in the vicinity of the fire. The tunnel height at the fire location was 4.7 m. The objectives of the test series were to investigate: (a) fire development in HGV cargo loads, (b) the influence of longitudinal ventilation on fire HRR and growth rate, (c) production of toxic gases, (d) fire spread between vehicles, (e) fire fighting possibilities and (f) temperature development at the tunnel ceiling and along the tunnel.

Peak heat release rates in the range of 67 – 202 MW and peak gas temperatures in the range of 1250 – 1350 °C were measured using non-hazardous cargoes. Prior to these tests this high temperature level had only been observed in tests with liquid fires in tunnels. These tests show that ordinary trailer loads can generate the same level of heat release rate and ceiling temperatures as a tanker fire. The fire development in all the tests was very fast, despite a relatively small ignition source. The peak heat release rates were reached between 8 and 18 minutes after ignition.

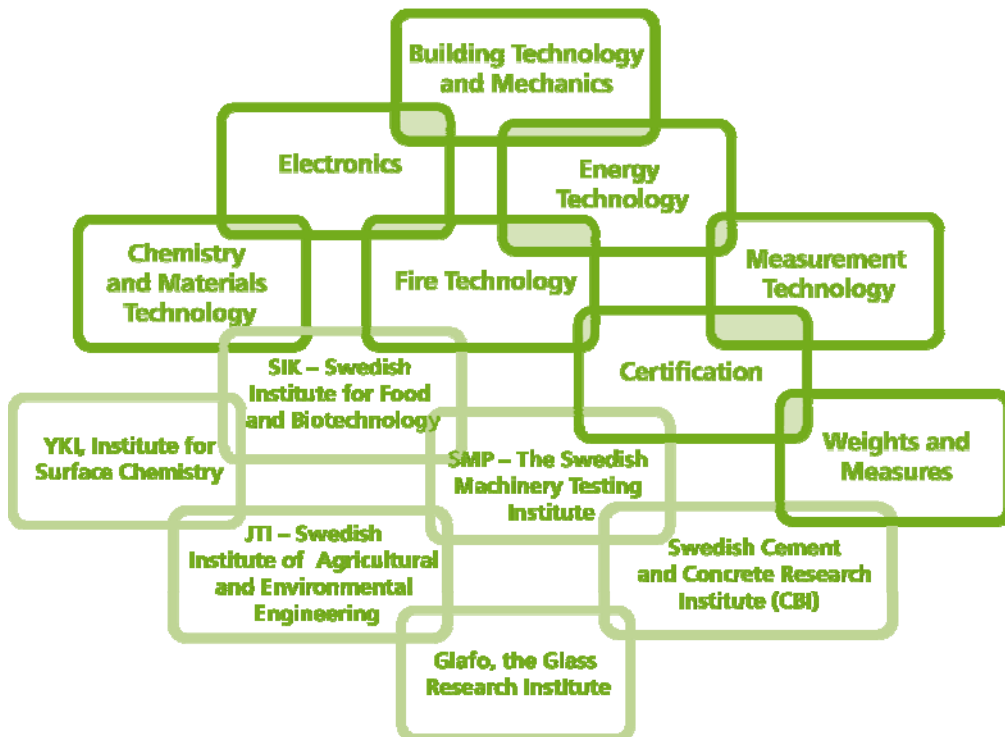
Table B8 The test program for the Runehamar tests [44-45].

Test nr.	Fire source	Type of ventilation	Target	E_{tot}	u	T_0	Q_{max}	T_{max}	H_f^*	b_{fo}^*
				GJ	m/s	°C	MW	°C	m	
1	wood pallets, PE plastic pallets, tarpaulin	LTV	32 wood pallets and 6 PE pallets	242	2.7	12	202	1365	3.9	3.16
2	wood pallets, PUR mattresses, tarpaulin	LTV	20 wood pallets and 20 PUR mattresses	141	2.7	11	157	1282	3.9	3.16
3	Furniture, fixtures, tarpaulin	LTV	Upholstered sofa and arm rest on pallets	131	2.7	9.5	119	1281	3.9	3.16
4	paper cartons with interiors, polystyrene cups wood pallets, tarpaulin	LTV	No target	62	2.7	11	67	1305	3.9	3.16

*based on estimation of the authors

SP Technical Research Institute of Sweden

Our work is concentrated on innovation and the development of value-adding technology. Using Sweden's most extensive and advanced resources for technical evaluation, measurement technology, research and development, we make an important contribution to the competitiveness and sustainable development of industry. Research is carried out in close conjunction with universities and institutes of technology, to the benefit of a customer base of about 9000 organisations, ranging from start-up companies developing new technologies or new ideas to international groups.



SP Technical Research Institute of Sweden

Box 857, SE-501 15 BORÅS, SWEDEN

Telephone: +46 10 516 50 00, Telefax: +46 33 13 55 02

E-mail: info@sp.se, Internet: www.sp.se

www.sp.se

Fire Technology

SP Report 2010:51

ISBN 91-85303-82-8

ISSN 0284-5172

More information about publications published by SP: www.sp.se/publ